Andreas Kleinbichler

Periodic Structures of Metallic Nanoparticles

Diplomarbeit

zur Erlangung des akademischen Grades eines Magisters

an der Naturwissenschaftlichen Fakultät der
Karl-Franzens-Universität Graz

Betreuer: Ao.Univ.-Prof. Mag. Dr. Ulrich Hohenester

Institut für Physik
Fachbereich Theoretische Physik

Abstract

The interaction of light with nanostructures is of high interest in todays research and future applications. For metallic nanoparticles this interaction is based on the principle of surface plasmons, which are changes in the density oscillations of the conduction electrons due to the light excitation.
The subject of this thesis is to derive a framework to describe the optical properties of two dimensional gratings of identical metallic nanoparticles. The approach used is to calculate one particle with the electromagnetic influence of the array, due to the use of Green's functions.
First the theoretical idea is described for the simulation of the an nanostructured array. For the simulation the MNPBEM toolbox for Matlab [1] is used which uses the boundary element method [2] to calculate the electromagnetic potentials and in the following the surface currents and charges. With these theoretical and computational foundations, the far field scattering and extinction cross sections are calculated for different array sizes (number of particles) and grating orders (interparticle distances).
After that, the angle dependence of the incident light excitation is incorporated into the simulation. This shows the change of the grating orders due to different light excitations.
Both simulations are carried out for two different particle shapes, showing the dependency of the radiation on the plasmons resonance frequency, which is determined by the particles geometry.
Finally, the multipole expansion of the Green's functions is discussed, which improves the calculation of the spectra with the MNPBEM, meaning that the computing time can be reduced for large arrays rendering the simulation more efficient.

Contents

1. Introduction

A current field of strong interest are metal nanoparticles, which are usually 10 to $100nm$ in size. The reason for the extensive studies of the electrodynamic properties of those particles are their surface plasmon modes. Such nanoparticles can be seen as resonators for surface plasmons which can be characterized by density oscillations of the conduction electrons of the metal. If excited resonantly the oscillation amplitude can overcome the excitation amplitude by orders of magnitude which, for metal nanoparticles, means a strong enhancement of the local electromagnetic field in comparison to the exciting field [3]. The optical properties exhibited by these particles are also strongly dependent on their size and geometrical shape in addition to their material properties.

The effects of metal nanoparticles are not a feature of the present century. The most notable historical example is the roman Lycurgus cup, in figure 1.1, from the fourth century A.D. [4]. Due to plasmonic excitation of the metal nanoparticles suspended in the glass the cup scatters and absorbs the short wavelength of the spectrum. The same principle is involved in medieval church windows, where the colors arise from nanoparticles of different metals embedded in the glass.

Due to new methods for constructing nanoscale structures, it has been made possible to build and test ultrasmall plasmonic devices and circuits. These methods include rather complicated and expensive schemes like electron beam lithography but more simpler ones like chemical condensation or thermally vacuum deposited metal island films and so on.
Modern applications of metal nanoparticles have a wide range, from medicine to electronics. For example slot waveguides which can significantly boost the speed of computer chips where dielectric waveguides deliver optical signals to an array of plasmonic switches called plasmonsters [4], and then distributing the signals to transistors. The plasmonsters are composed of slot waveguides that measure $100nm$ across at their

Figure 1.1.: Roman Lycurgus cup held in the British museum. When a light source is placed inside the the green goblet, it appears red.(picture take from the British Museum)

broadest points and only $20nm$ across at the intersections.
Another example is subwavelength spatial confinement of light at dimensions down to less than a tenth of the free-space wavelength due to plasmonic components. This gives rise to the large and highly tunable dielectric permittivities for metals, especially near their plasmon resonances. Ultimately it may be possible to employ plasmonic components to form the building blocks of a chip-based nanophotonic device technology that is scaleable essentially to molecular dimensions, with potential imaging, spectroscopy and interconnection applications in computing, communication and chemical/biological detection.

In this context it is important to have computational tools to simulate the plasmonic behavior of such metal nanoparticle structures, to be able to predict and explain experimental findings which will be the subject of this thesis. The aim is to use the existing MNPBEM toolbox [1] and modify it so that one can describe the plasmonic effects of optically excited periodic arrays of metal nanoparticles. Special emphasis is placed on the simulation of the scattering for different interparticle distances and different incidence angles of the light excitation. Furthermore it is intended to optimize the simulation in terms of computing time which is dependent on the number of particles in the structure.

This thesis is structured into six chapters. In the first two chapters the theoretical foundations are presented. Chapter 2 establishes a framework of how to calculate electromagnetic potentials and Maxwell's equations at interfaces, Green's functions and electromagnetic radiation. Chapter 3 is dedicated to the illustration and theoretical description of plasmons. In chapter 4 the approach to compute the electromagnetic response of a periodic array of metallic nanoparticles is formulated. Chapter 5 is devoted to the simulation program, MNPBEM which is used for the following calculations. The last chapter 6 shows the results of the simulations done in the course of this thesis, and gives a brief discussion about the modifications implemented to boost efficiency.

2. Theory

2.1. Maxwell's equations

Maxwell's equations are the fundamental mathematical tool for describing any phenomena concerning electromagnetism. In 1864 Maxwell published his famous formulas which describe the dynamic of the electric field $\mathbf{E}(\mathbf{r}, t)$ and the magnetic induction $\mathbf{B}(\mathbf{r}, t)$. These equations read in their macroscopic form and in Gaussian units [5]

$$\nabla \cdot \mathbf{D}(\mathbf{r}, t) = 4\pi\rho(\mathbf{r}, t), \tag{2.1a}$$

$$\nabla \cdot \mathbf{B}(\mathbf{r}, t) = 0, \tag{2.1b}$$

$$\nabla \times \mathbf{H}(\mathbf{r}, t) = \frac{4\pi}{c}\,\mathbf{j} + \frac{1}{c}\frac{\partial\,\mathbf{D}(\mathbf{r}, t)}{\partial t}, \tag{2.1c}$$

$$\nabla \times \mathbf{E}(\mathbf{r}, t) = -\frac{1}{c}\frac{\partial\,\mathbf{B}(\mathbf{r}, t)}{\partial t}, \tag{2.1d}$$

where $\mathbf{D} = \epsilon\,\mathbf{E}$ is the dielectric displacement for linear and isotropic media, ρ is the free charge density, $\mathbf{j}$ is the electric current density, c is the speed of light and $\mathbf{B} = \mu\,\mathbf{H}$ the magnetic field . In the following the permittivity ϵ is assumed to be uniform for each medium, and because we are only interested in light at optical frequencies we set $\mu = 1$.

The meaning of these equations is rather significant. Equation (2.1a), the Gauss law, states that electric charges are the sources and sinks of the electric field. Equation (2.1b) is the magnetic analogon to the Gauss law and states that the magnetic field is source free, hence there are no magnetic monopoles. The equations (2.1c) and (2.1d), Ampére's and Faraday's law, describe that electric fields induce a curl magnetic field and vice versa.

Because we will deal only with effects linear in the $\mathbf{E}$ and $\mathbf{B}$ fields, in the following it is sufficient to use time harmonic fields which can be acquired through Fourier transform

of the time dependent fields [6], shown in A.1

$$\mathbf{E}(\mathbf{r},t) = \mathbf{E}(\mathbf{r})\,\mathrm{e}^{-i\omega t} \quad , \quad \mathbf{B}(\mathbf{r},t) = \mathbf{B}(\mathbf{r})\,\mathrm{e}^{-i\omega t}\,. \tag{2.2}$$

The Maxwell equations with no sources present ($\rho = 0$ and $\mathbf{j} = 0$) now read

$$\nabla \cdot \mathbf{D}(\mathbf{r},\omega) = 0, \qquad \nabla \cdot \mathbf{B}(\mathbf{r},\omega) = 0, \tag{2.3a}$$

$$\nabla \times \mathbf{E}(\mathbf{r},\omega) = i\frac{\omega}{c}\,\mathbf{B}(\mathbf{r},\omega), \qquad \nabla \times \mathbf{B}(\mathbf{r},\omega) = -i\frac{\omega}{c}\,\mathbf{D}(\mathbf{r},\omega). \tag{2.3b}$$

Next we take the curl of Faraday's and Ampére's law (2.3b) which leads us to six second order differential equations called the Helmholtz wave equations (see A.2)

$$(\nabla^2 + \epsilon k^2)\,\mathbf{E}(\mathbf{r},\omega) = 0, \tag{2.4a}$$

$$(\nabla^2 + \epsilon k^2)\,\mathbf{B}(\mathbf{r},\omega) = 0, \tag{2.4b}$$

with $k = \frac{\omega}{c}$ being the wavenumber. We are able to uncouple and reduce the number of equations by introducing the scalar and vector potential. First we substitute

$$\mathbf{B} = \nabla \times \mathbf{A}, \tag{2.5a}$$

$$\mathbf{E} = -\nabla\Phi + ik\,\mathbf{A}, \tag{2.5b}$$

into the Maxwell equations (2.3a) and (2.3b). For the second step we need to choose the Lorentz gauge condition, which leaves the fields $\mathbf{E}$ and $\mathbf{B}$ unchanged [7]

$$\nabla \cdot \mathbf{A} - ik\epsilon\Phi = 0. \tag{2.6}$$

With this condition we have uncoupled (2.4a) and (2.4b) by expressing the scalar potential through the divergence of the vector potential. Now this leads to the Helmholtz equations for the harmonic scalar and vector potentials (with sources ρ and $\mathbf{j}$ again included), two wave equations that are equivalent to Maxwell's equations

$$(\nabla^2 + \epsilon k^2)\Phi(\mathbf{r},\omega) = -4\pi\rho(\mathbf{r},\omega), \tag{2.7a}$$

$$(\nabla^2 + \epsilon k^2)\,\mathbf{A}(\mathbf{r},\omega) = -\frac{4\pi}{c}\,\mathbf{j}(\mathbf{r},\omega). \tag{2.7b}$$

2.2. Green's function

An important tool throughout the next chapters will be the Green's function which was introduced by George Green in 1828. It is a impulse response of an inhomogeneous differential equation, with specific boundary conditions. The Green's function is an important concept of field theory because it connects an electromagnetic field to a point source.

2.2.1. Mathematical basis and derivation

The mathematical foundation will be given by the example of a general, inhomogeneous equation [6]

$$\mathfrak{L}\,\mathbf{A}(\mathbf{r}) = \mathbf{B}(\mathbf{r}). \tag{2.8}$$

Here $\mathfrak{L}$ is a linear operator acting on a vector field $\mathbf{A}$, which describes the response of the system, and with $\mathbf{B}$ being the inhomogeneity. For linear differential equations the general solution is equal to the sum of the complete homogeneous solution plus a particular inhomogeneous solution. When the homogeneous solution is known, one can just solve for a inhomogeneity that is zero everywhere except at one point, which is the Dirac delta function $\delta(\mathbf{r}-\mathbf{r}')$,

$$\mathfrak{L}G(\mathbf{r},\mathbf{r}') = \delta(\mathbf{r}-\mathbf{r}'). \tag{2.9}$$

If such a G exists for a certain $\mathfrak{L}$, then (2.9) can be multiplied on both sides with $\mathbf{B}(\mathbf{r}')$ and integrated over a volume V, which gives

$$\int_V \mathfrak{L}G(\mathbf{r},\mathbf{r}')\,\mathbf{B}(\mathbf{r}')dV' = \int_V \mathbf{B}(\mathbf{r}')\delta(\mathbf{r},\mathbf{r}')dV'. \tag{2.10}$$

The right hand side reduces to $\mathbf{B}(\mathbf{r})$, so (2.8) can be used and by taking out the operator $\mathfrak{L}$ (not always valid) it follows

$$\mathbf{A}(\mathbf{r}) = \int_V G(\mathbf{r},\mathbf{r}')\,\mathbf{B}(\mathbf{r}')dV'. \tag{2.11}$$

So the solution is the integral of the Green's function multiplied with the inhomogeneity over the source volume.

For the case of a static electrical point charge with certain boundary conditions the Poisson equation

$$\nabla^2 G(\mathbf{r}, \mathbf{r}') = -4\pi\delta(\mathbf{r} - \mathbf{r}') \tag{2.12}$$

has to be solved. Here G is given by the static Green's function

$$G(\mathbf{r}, \mathbf{r}') = \frac{1}{|\,\mathbf{r} - \mathbf{r}'\,|}. \tag{2.13}$$

This leads to an expression for the electric potential

$$\Phi(\mathbf{r}) = \epsilon \int_V \rho(\mathbf{r}')G(\mathbf{r} - \mathbf{r}')dV'. \tag{2.14}$$

In the previous section the Helmholtz equation was introduced which has the form

$$[\nabla^2 + k^2]f(\mathbf{r}) = -g(\mathbf{r}). \tag{2.15}$$

To derive the scalar Green's function $G(\mathbf{r}, \mathbf{r}')$ for the Helmholtz equation, the source term $g(\mathbf{r})$ will be taken to be a single point source $\delta(\mathbf{r} - \mathbf{r}')$. From this one gets

$$[\nabla^2 + k^2]G(\mathbf{r}, \mathbf{r}') = -\delta(\mathbf{r} - \mathbf{r}'). \tag{2.16}$$

In this equation $\mathbf{r}'$ denotes the location of the source point and $\mathbf{r}$ designates the point where the fields are to be evaluated. In free space the only physical solutions to this equation are [8]

$$G(\mathbf{r}, \mathbf{r}') = \frac{e^{\pm ik|\,\mathbf{r} - \mathbf{r}'\,|}}{|\,\mathbf{r} - \mathbf{r}'\,|}. \tag{2.17}$$

The derivation of (2.17) is shown in A.3. The denominator with the plus sign represents spherical outgoing waves and the minus sign stands for spherical waves that converge towards the origin.
In the following the vector potential can be calculated be inserting (2.17) in

$$\mathbf{A}(\mathbf{r}) = \mu \int_V \mathbf{j}(\mathbf{r}')G(\mathbf{r}, \mathbf{r}')dV'. \tag{2.18}$$

A similar expression holds for the scalar potential.

2.2.2. Multipole expansion

In this section we will introduce how to expand the Green's function in terms of orthonormal functions, which will be used in the later chapters [5]. To start, we examine the expansion of a potential at a point $\mathbf{r}$ generated by a point source at $\mathbf{r}'$

$$\frac{1}{|\,\mathbf{r}-\mathbf{r}'\,|} = \sum_{l=0}^{\infty} \frac{r_<^l}{r_>^{l+1}} P_l(\cos\gamma). \tag{2.19}$$

Where $r_<$ ($r_>$) is the smaller (greater) of $|\,\mathbf{r}\,|$ and $|\,\mathbf{r}'\,|$, and γ is the angle between $\mathbf{r}$ and $\mathbf{r}'$. If we now use the addition theorem of spherical harmonics, the Legendre polynomial $P_l(\cos\gamma)$ can be expressed as a product of the spherical harmonics $Y_{l,m}$ of the angles Θ, Φ and Θ', Φ'. Together with equation (2.19), we get the multipole expansion for the Green's function of a static point charge

$$\frac{1}{|\,\mathbf{r}-\mathbf{r}'\,|} = 4\pi \sum_{l=0}^{\infty} \frac{1}{2l+1} \frac{r_<^l}{r_>^{l+1}} \sum_{m=-l}^{l} Y_{l,m}^*(\Theta',\Phi') Y_{l,m}(\Theta,\Phi). \tag{2.20}$$

In the following we will need a spherical wave expansion for outgoing waves, which fulfills equation (2.16) and has the solution (2.17). The expansion for G follows from [5]

$$G(\mathbf{r},\mathbf{r}') = \sum_{l,m} g_l(\mathbf{r},\mathbf{r}') Y_{l,m}^*(\Theta',\Phi') Y_{l,m}(\Theta,\Phi). \tag{2.21}$$

Where $Y_{l,m}$ and $Y_{l,m}^*$ are the spherical harmonics and its complex conjugate, respectively. Here we have separated the Green's function into a radial and angular part. After substituting into (2.16) we get the equation

$$\left[\frac{d^2}{dr^2} + \frac{2}{r}\frac{d}{dr} + k^2 - \frac{l(l+1)}{r^2}\right] g_l = -\frac{1}{r^2}\delta(\mathbf{r}-\mathbf{r}'). \tag{2.22}$$

The solution to this equation which has to be finite at the origin and behaves like a outgoing wave as $r \to \infty$, is

$$g_l(\mathbf{r}-\mathbf{r}') = A j_l(k\,\mathbf{r}_<) h_l^{(1)}(k\,\mathbf{r}_>), \tag{2.23}$$

with $j_l(k\,\mathbf{r}_<)$ being the spherical Bessel functions and $h_l^{(1)}(k\,\mathbf{r}_>)$ the spherical Hankel functions. The correct behavior of g_l at the discontinuity of the derivation is assured if

$A = ik$. Hence, the multipole expansion of the retarded Green's function reads

$$\frac{e^{ik|\,\mathbf{r}-\mathbf{r}'\,|}}{4\pi|\,\mathbf{r}-\mathbf{r}'\,|} = ik\sum_{l=0}^{\infty} j_l(kr_<)h_l^{(1)}(kr_>)\sum_{m=-l}^{l} Y_{l,m}^*(\Theta',\Phi')Y_{l,m}(\Theta,\Phi). \tag{2.24}$$

2.3. The Boundary element method

With the Boundary Element Method (BEM) we express the fields inside a homogeneous medium in terms of the interface sources, at a sharp boundary to a different homogeneous medium. We then use the continuity of the potential and the electric displacement, together with the boundary conditions for the surface derivatives, to calculate them self-consistently [2].

2.3.1. The quasi-static approximation

If we are dealing with particles whose sizes are much smaller than the wavelength of the incident light, we can disregard retardation effects and set the wave number $k = 0$ in equation (2.7a). Another consequence is that due to the Lorenz gauge the vector potential $\mathbf{A}$ vanishes. Therefore the Helmholtz equation becomes

$$\nabla^2\Phi = -4\pi\rho \tag{2.25}$$

Without external charges this formula reduces to the Laplace equation

$$\nabla^2\Phi = 0 \tag{2.26}$$

This differential equation can be solved by the Green's function, in this case the quasi-static Green's function

$$G(\mathbf{r}-\mathbf{r}') = \frac{1}{|\,\mathbf{r}-\mathbf{r}'\,|}, \tag{2.27a}$$

$$\Downarrow$$

$$\nabla^2 G(\mathbf{r},\mathbf{r}') = -4\pi\delta(\mathbf{r}-\mathbf{r}'). \tag{2.27b}$$

Normally we have to take into account the volume of the system, but since we are dealing with homogeneous media ($\epsilon(\omega)$ is a constant inside each medium) we can make

use of the divergence theorem (Gauss's theorem) and switch from a volume integration to a surface integration, writing the integral equation for the potential [9]

$$\Phi(\mathbf{r}) = \oint_{\partial\Omega} \sigma(\mathbf{s}')G(\mathbf{r},\mathbf{s}')da' + \Phi_{ext}(\mathbf{r}). \tag{2.28}$$

This fulfills the Poisson equation everywhere except on the boundaries $\partial\Omega$ between the media. Now we need to take the boundaries into account by considering the electromagnetic boundary conditions for the potentials

$$\hat{\mathbf{n}} \cdot (\epsilon_1 \nabla\Phi_1 - \epsilon_2 \nabla\Phi_2) = 0, \tag{2.29}$$

see A.5. Therefore we need to calculate the normal derivative $\hat{\mathbf{n}} \cdot \nabla\Phi$ for the potential (2.28). When this is done, we arrive at

$$\frac{\partial\Phi}{\partial n} = \int_{\partial\Omega} F(\mathbf{s},\mathbf{s}')\sigma(\mathbf{s}')da' \pm 2\pi\sigma(\mathbf{s}) + \frac{\partial\Phi_{ext}}{\partial n} \quad , \quad F(\mathbf{s},\mathbf{s}') = \hat{\mathbf{n}} \cdot \nabla G(\mathbf{r} - \mathbf{s}'). \tag{2.30}$$

An analytic solution for equation (2.30) was found by Gustav Mie [10] for a spherical geometry. In order to generalize to arbitrary boundaries we must take a leave from the surface integral $\partial\Omega$, and instead discretize the surface into small boundary elements $\partial\Omega_i$. This changes equation (2.30) to

$$\left(\frac{\partial\Phi}{\partial n}\right)_i = \sum_j F_{ij}\sigma_j \pm 2\pi\sigma_i + \left(\frac{\partial\Phi_{ext}}{\partial n}\right). \tag{2.31}$$

Using the boundary conditions (2.29) and matrix notation[1], equation (2.31) leads to a expression for the surface charge σ:

$$\boldsymbol{\sigma} = -[\hat{\boldsymbol{\Lambda}} + \hat{\mathbf{F}}]^{-1} \frac{\partial\Phi_{ext}}{\partial n} \quad , \quad \hat{\boldsymbol{\Lambda}} = 2\pi \frac{\epsilon_2 + \epsilon_1}{\epsilon_2 - \epsilon_1} \mathbb{1}. \tag{2.32}$$

So in the quasi-static approximation σ only depends on the material parameter $\hat{\boldsymbol{\Lambda}}$ and the surface derivative of the Green's function $\hat{\mathbf{F}}$. Inserting (2.32) back into (2.29) leads to the solution which gives the potential and electric field in every point in the two media.

[1] Φ, Φ_{ext} and σ are vectors of size N, $\hat{\mathbf{F}}$ is a $N \times N$ matrix

2.3.2. Solving the full Maxwell equations

If the characteristic length of the system under investigation is no longer sufficiently small compared to the wavelength of the exciting light, the quasi-static approximation loses legitimacy. This means that the full Maxwell equations have to be solved.
Because of the wavenumber $k \neq 0$, the vector potential $\mathbf{A}$ cannot be neglected anymore and the electromagnetic fields have to be computed from equations (2.5a) and (2.5b).
Now we are looking for a solution of the full Helmholtz equations (2.7a) and (2.7b) which we now write as

$$[\nabla^2 + k_j^2] G_j(\mathbf{r}, \mathbf{r}') = 4\pi\delta(\mathbf{r} - \mathbf{r}'). \tag{2.33}$$

The solution to this equation is the retarded Green's function G_j and similar to the quasi-static case, only the Green's function and its surface derivative will be used in the following

$$G_j = \frac{e^{ik_j|\,\mathbf{r}-\mathbf{r}'\,|}}{|\,\mathbf{r}-\mathbf{r}'\,|} \quad , \quad F_j = \hat{\mathbf{n}}_s \cdot \nabla_s G_j(|\mathbf{s} - \mathbf{s}'|) \tag{2.34}$$

the index j designating the medium[2].
Now the potentials can be written, similar to the quasi-static case, as integrals over the boundaries for each medium j:

$$\Phi(\mathbf{r}) = \int\limits_{\partial\Omega_j} G_j(\mathbf{r}, \mathbf{s}')\sigma_j(\mathbf{s}')da' + \Phi_{ext}(\mathbf{r}) \tag{2.35a}$$

$$\mathbf{A}(\mathbf{r}) = \int\limits_{\partial\Omega_j} G_j(\mathbf{r}, \mathbf{s}')\,\mathbf{h}_j(\mathbf{s}')da' + \mathbf{A}_{ext}(\mathbf{r}) \tag{2.35b}$$

These potentials (2.35a) and (2.35b) are solutions of the Helmholtz equations in different media. Here $\sigma_j(\mathbf{s}')$ and $\mathbf{h}_j(\mathbf{s}')$ are the surface charges and currents for each medium j. Φ_{ext} and $\mathbf{A}_{ext}$ are the external potentials, produced by an excitation (e.g. plane wave, dipole).
There are two important differences to the quasi-static approximation.
First, it is no longer in general possible for surface charges and currents to be identical at different sides of the boundary. Second, the external potentials inside the different media have to be chosen in such a way that they are only induced by sources directly

[2] with $k_j = k\sqrt{\epsilon_j}$

next to the particles boundaries. This means that sources act only on the boundary adjoint to the next dielectric medium.
For the next step the Maxwell boundary conditions need to be used. The tangential electric field and the normal magnetic induction are continuous at the boundaries and therefore Φ and $\mathbf{A}$ are also continuous. With the notation from [9] (considering two media, $j = 1, 2$)

$$\Phi_1 = G_{11}\sigma_1 + G_{12}\sigma_2 + \phi_1^{ext}, \tag{2.36a}$$
$$\Phi_2 = G_{21}\sigma_1 + G_{22}\sigma_2 + \phi_2^{ext}. \tag{2.36b}$$

Φ_1 and Φ_2 are the scalar potentials in and outside the particle boundaries, with Φ_j^{ext} being the external potential in each medium. G_{11} denotes the Green's function which connects points on the inner boundary, G_{22} on the outer boundary, and G_{12} and G_{21} connects points from the inner to the outer boundary and vice versa.
Because of the continuity, the potentials can be expressed as

$$G_1\sigma_1 = G_2\sigma_2 + \Delta\Phi_{ext}, \qquad G_1\,\mathbf{h}_1 = G_2\,\mathbf{h}_2 + \Delta\,\mathbf{A}_{ext}, \tag{2.37a}$$
$$\sigma_1 = G_1^{-1}(G_2\sigma_2 + \Delta\Phi_{ext}), \qquad \mathbf{h}_1 = G_1^{-1}(G_2\,\mathbf{h}_2 + \Delta\,\mathbf{A}_{ext}), \tag{2.37b}$$

with equations (2.37b) being the surface charges and currents for the inner the boundary respectively, where we used

$$G_1 = G_{11} - G_{21}, \quad \Delta\Phi_{ext} = \Phi_2^{ext} - \Phi_1^{ext},$$
$$G_2 = G_{22} - G_{12}, \quad \Delta\,\mathbf{A}_{ext} = \mathbf{A}_2^{ext} - \mathbf{A}_1^{ext},$$

with $\mathbf{A}_j^{ext}$ being the external vector potential.
Through the continuity of the tangential magnetic field and the normal electric displacement, which will be discussed in the appendix A.6, we finally arrive at the surface charge and currents on the outside of the boundary

$$\sigma_2 = G_2^{-1}\Sigma^{-1}(D_e + ik\mathbf{n}(L_1 - L_2)\Delta^{-1}\vec{\alpha}, \tag{2.38a}$$
$$\mathbf{h}_2 = G_2^{-1}\Delta^{-1}(ik\mathbf{n}(L_1 - L_2)G_2\sigma_2 + \vec{\alpha}. \tag{2.38b}$$

2.4. Radiation

A important tool for the following chapters will be the emission of electromagnetic radiation due to localized charge or current distributions [5]. For charge and current distributions varying in time we can use a Fourier analysis to deal with each component separately. We can therefore assume for these distributions a harmonic time dependence[3]

$$\begin{aligned} \rho(\mathbf{r},t) &= \rho(\mathbf{r})e^{-i\omega t}, \\ \mathbf{j}(\mathbf{r},t) &= \mathbf{j}(\mathbf{r})e^{-i\omega t}. \end{aligned} \tag{2.39}$$

Because of (2.39) the solution for the vector potential $\mathbf{A}$ becomes

$$\mathbf{A}(\mathbf{r}) = \frac{\mu_0}{4\pi}\int\limits_V \mathbf{j}(\mathbf{r}')\frac{e^{ik|\,\mathbf{r}-\mathbf{r}'\,|}}{|\,\mathbf{r}-\mathbf{r}'\,|}dV. \tag{2.40}$$

With the wavenumber $k = \sqrt{\epsilon}\frac{\omega}{c}$ and the harmonic time dependence has been omitted. If the current distribution is known, the fields can be calculated with equation (2.40). If d represents the source dimension and $\lambda = \frac{2\pi c}{\omega}$ is the wavelength, we will assume that d is very small compared to ω. Now one has to consider the behavior of the fields in the three different regions around the source

near zone:	$d \ll r \ll \lambda$
intermediate zone:	$d \ll r \sim \lambda$
far zone:	$d \ll \lambda \ll r$

In the near zone the fields have the character of static radial fields which change with distance. This means that $kr \ll 1$ in the exponent of equation (2.40), hence it can be set to 1. The vector potential then takes the form

$$\mathbf{A}(\mathbf{r}) = \frac{\mu_0}{4\pi}\int\limits_V \frac{\mathbf{j}(\mathbf{r}')}{|\,\mathbf{r}-\mathbf{r}'\,|}dV. \tag{2.41}$$

In the far zone the field is orthonormal to the radius vector and falls off as r^{-1}. Here $kr \gg 1$ and the exponent in equation (2.40) is oscillating heavily which dominates the vector potential. Therefore we are able to use the following approximation shown in

[3] we take the real part of this expression to get physical quantities

A.7

$$| \mathbf{r} - \mathbf{r}' | \simeq r - \hat{\mathbf{n}} \cdot r'. \tag{2.42}$$

Here $\hat{\mathbf{n}}$ is the unit vector in the direction of $\mathbf{r}$. With this, equation (2.40) becomes in leading order

$$\lim_{kr\to\infty} \mathbf{A}(\mathbf{r}) = \frac{\mu_0}{4\pi} \frac{e^{ikr}}{r} \int\limits_V \mathbf{j}(\mathbf{r}') e^{-ik\,\hat{\mathbf{n}}\,\mathbf{r}'} dV. \tag{2.43}$$

Hence, the vector field in the far zone behaves like a spherical wave with a angular dependence. These radiation fields in the far zone are the ones we will be interested in later.

3. Plasmons

The interaction of metals with light is mainly determined by the free conducting electrons of the metal. At optical frequencies the free electron gas can sustain charge oscillations on the surface of the metallic medium, called surface plasmons. These quasi particles can be described classically by a complex dielectric function that contains the optical response of the metal, according to the Drude-Sommerfeld theory. A special case are the particle plasmons which occur for metallic particles, typically smaller than the wavelength of the exciting light [6].

3.1. Dielectric function of metals

As mentioned above, the optical properties of the metals are determined mainly by the free movement of the conduction electrons within the bulk, and are described by the complex, frequency dependent dielectric function. To illustrate, we can assume that, due to an electromagnetic field the electrons are displaced by a vector $\mathbf{r}$ which leads to a dipole moment $\boldsymbol{\mu} = e\,\mathbf{r}$. On a macroscopic level we get the polarization $\mathbf{P} = n\boldsymbol{\mu}$, with n being the number of electrons in the unit volume. A way to obtain $\mathbf{P}$ is to solve the equation of motion of the electrons under influence of the external field. To do so, we use the Drude-Sommerfeld theory for the free electron gas with the equation of motion

$$m\frac{\partial^2 \mathbf{r}}{\partial t^2} + m\gamma\frac{\partial \mathbf{r}}{\partial t} = e\,\mathbf{E}_0\,e^{-i\omega t}, \tag{3.1}$$

where γ is the damping term, m and e are the electron mass and charge, respectively. The external field has the amplitude $\mathbf{E}_0$ and the frequency ω. We solve equation (3.1) by using the ansatz $\mathbf{r}(t) = \mathbf{r}_0\,e^{-i\omega t}$ and arrive at the Drude dielectric function

$$\epsilon(\omega) = 1 - \frac{\omega_p}{\omega^2 + i\gamma\omega}, \tag{3.2}$$

with ω_p being the plasma frequency. A negative real part of the dielectric constant ϵ, as it is the case for metals, has the consequence that it can only travel a short distance into the metal because, the imaginary part of the refractive index $n = \sqrt{\epsilon}$ becomes strongly negative.

3.2. Surface plasmons

Surface plasmons are located at plane interfaces between metals and dielectrics. When we assume the interface in the xy-plane, where ϵ_1 is real representing the dielectric and ϵ_2 is complex characterizing the metal, we need to use Maxwell's theory to investigate the interface, and solve the Helmholtz wave equation (2.4a)

$$\left(\nabla^2 + \epsilon(\mathbf{r}, \omega)\frac{\omega^2}{c^2}\right)\mathbf{E}(\mathbf{r}, \omega) = 0, \tag{3.3}$$

with $\epsilon(\mathbf{r}, \omega) = \epsilon_1$ for $z < 0$ and $\epsilon(\mathbf{r}, \omega) = \epsilon_2$ for $z > 0$. If we split the electric field into a parallel component called p-polarized and a perpendicular component called s-polarized with respect to the incidence plane, it can be shown that there exists no solution of the Helmholtz equation (2.4a) for the s-polarized case [6]. Hence, only p-polarized fields E_j are of interest, where $j = 1, 2$ denotes the medium

$$\mathbf{E}_j = \begin{pmatrix} E_{j,x} \\ 0 \\ E_{j,z} \end{pmatrix} e^{i(k_x x + k_{j,z} z - \omega t)}. \tag{3.4}$$

Because of the fact that the parallel component of the wave vector is conserved the following relation can be used

$$k_x^2 + k_{j,z}^2 = \epsilon k^2, \tag{3.5}$$

where $k = 2\pi/\lambda$. By using equation (2.3b) and considering that both half spaces are source free we arrive at

$$k_x E_{j,x} + k_{j,z} E_{j,z} = 0, \tag{3.6}$$

which, by inserting into equation (3.4), leads us to

$$\mathbf{E}_j = E_{j,x} \begin{pmatrix} 1 \\ 0 \\ -k_x/k_{j,z} \end{pmatrix} e^{i(k_x x + k_{j,z} z - \omega t)}. \tag{3.7}$$

After the fields have been defined, the boundary conditions from A.4 have to be used which then read

$$\begin{aligned} E_{1,x} - E_{2,x} &= 0, \\ \epsilon_1 E_{1,z} - \epsilon_2 E_{2,z} &= 0. \end{aligned} \tag{3.8}$$

A solution of equations (3.6) and (3.8) requires either $k_x = 0$, which indicates that their is no propagation along the surface, or

$$\epsilon_1 k_{2,z} - \epsilon_2 k_{1,z} = 0. \tag{3.9}$$

Taking this equation together with (3.6) leads us to the dispersion relations for the parallel and the normal component of k, respectively

$$k_x^2 = \frac{\epsilon_1 \epsilon_2}{\epsilon_1 + \epsilon_2} k^2 = \frac{\epsilon_1 \epsilon_2}{\epsilon_1 + \epsilon_2} \frac{\omega^2}{c^2}, \tag{3.10}$$

$$k_{j,z}^2 = \frac{\epsilon_j^2}{\epsilon_1 + \epsilon_2} k^2. \tag{3.11}$$

For interface waves that propagate along the interface we need k_x^2 to be real. To achieve "bound" solutions, $k_{j,z}$ has to be imaginary in both media, thus confining it to the surface and preventing it from traveling into the media. In order to fulfill these conditions, we need the following conditions for the dielectric functions

$$\epsilon_1(\omega) \cdot \epsilon_2(\omega) < 0, \tag{3.12}$$

$$\epsilon_1(\omega) + \epsilon_2(\omega) < 0. \tag{3.13}$$

From this it follows that one dielectric function has to be negative with an absolute value greater than the other one. Metals and noble metals display such dielectric functions and therefore surface plasmons exist in these materials.

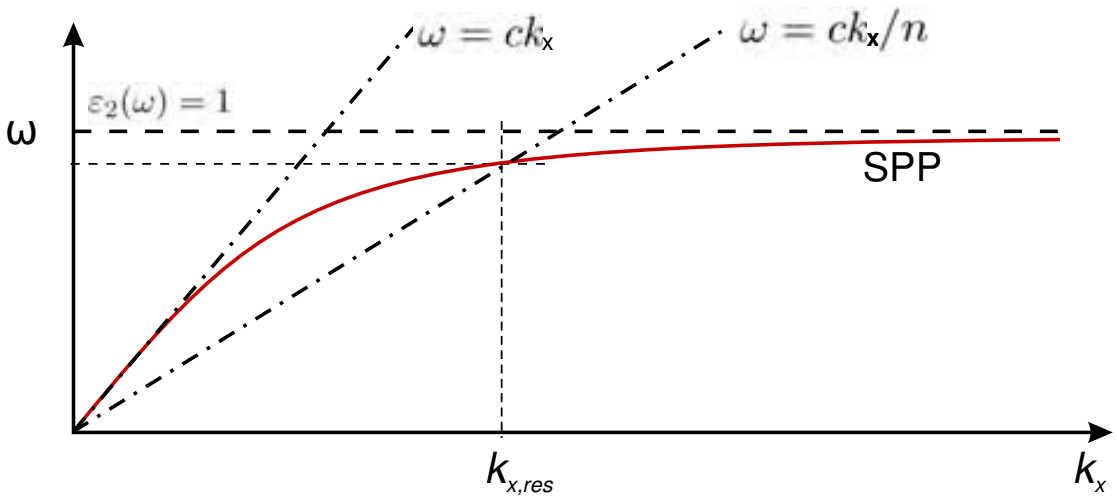

Figure 3.1.: Dispersion relation for a interface between metal and air with the light line in free space and the tilted light line in a dielectric. Because the dispersion line of the surface plasmon polariton (SPP) dose not cross the light line in air, no plasmon is excited. But the dispersion line crosses the tilted light line when we have a dielectric medium, and thus a SPP can be excited with a resonance at the crossing point $k_{x,res}$.

As we can see in figure 3.1 only at an interface between metal and a dielectric medium is it possible to excite a surface plasmon because the energy-momentum conservation has to be fulfilled. For $\omega = ck_x$ the momentum contribution of the incident light is to small, but $\omega = ck_x/n$ has a strong enough contribution.
The solution of tilting the light line can be achieved by sending the exciting wave through a optically denser medium and essentially slowing the incident light down. This can be accomplished with two experimental configuration, the Otto configuration and the Kretschmann configurations shown in figure 3.2.

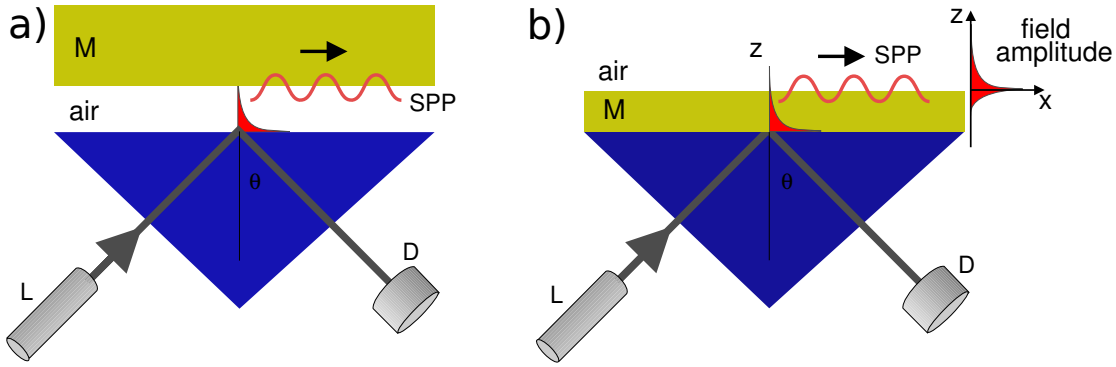

Figure 3.2.: a) The Otto configuration uses total reflection at the prism-air interface to generate an evanescent field which excites a SPP in the metal above. Here it is crucial to control the air slit optimally at some order of λ. b) The Kretschmann configuration has a total reflection at the prism-metal interface which generates a evanescent field in the metal that excites the SSP on the opposite site of the metal film [6].

3.3. Particle plasmons

As we have discussed above, plasmons arise from density oscillations of the conducting electrons due to the exciting electromagnetic fields. These can not only be induced in planar surfaces, but also metallic nano particles, provided they are smaller than the exciting light wave length. The free electron gas in the particles becomes polarized and restored by the ions of the background which form a plasmonic oscillation depicted in figure 3.3. These particle plasmons will be used in the following discussions and simulations.

Figure 3.3.: Due to a electromagnetic wave the whole particle gets polarized. The particle behaves like a oscillator with a resonance frequency dependent on the metal, the size and the geometry of the particle [11].

4. Periodic structures

4.1. Extension to periodic structures of nanoparticles

As discussed in the previous chapters, through the use of the Boundary Element Method (BEM) for the full Maxwell equations it is possible to calculate the surface charges and currents ((2.37b), (2.38a) and (2.38b)) and furthermore the electro-magnetic fields of a metallic nanoparticle. The question that will be the issue of this chapter is, how can a periodic array of nanoparticles of arbitrary size be simulated efficiently?
It is certainly possible to simulate every single particle of a specific array, i.e. to calculate each of the surface charges and currents with BEM and to evaluate the electromagnetic field at some point in space. However, such an approach to this problem will reach numerical limitations, because, we need to invert $N \times N$ matrices[1] in order to calculate the surface charges and currents [1]. It is obvious that the computing time will go up cubicly with increasing number of particles. Thus, for large arrays (e.g. $n_{particles} > 3$) it takes very long to compute the entire particle array.
In the following discussion we will show a way to deal with the whole periodic structure as a whole. First, through some modifications of the Green's function matrices that are used in the BEM, a lot of calculations we would have to carry out otherwise will become obsolete, which yields in a massive time saving. In a second step, another way to calculate the matrices for particles at far distances will be introduced, which yields in additional saving of time.

4.1.1. Modification of the Green's function

As mentioned in chapter 2, what is needed to calculate the surface charges and currents is the potential of a given excitation and the Green's function on the in and out side of

[1] N is the number of surface elements

the particle boundaries. The basic idea in this approach is that it is not necessary to simulate every particle of a periodic structure, one can make use of the periodicity and the fact that the Green's function contains all information about the electromagnetic effect at a boundary and connects it to the other boundaries. Thus, it is possible to calculate one single particle with the influence of the entire array, by the addition of the sum of the boundary Green's function, of all other particles in the structure to the Green's function of the single particle under consideration[2],

$$G_j(\mathbf{r}, \mathbf{r}') \rightarrow G_{j,0}(\mathbf{r}, \mathbf{r}') + \sum_{i \neq 0} G_{j,i}(\mathbf{r}, \mathbf{r}'). \tag{4.1}$$

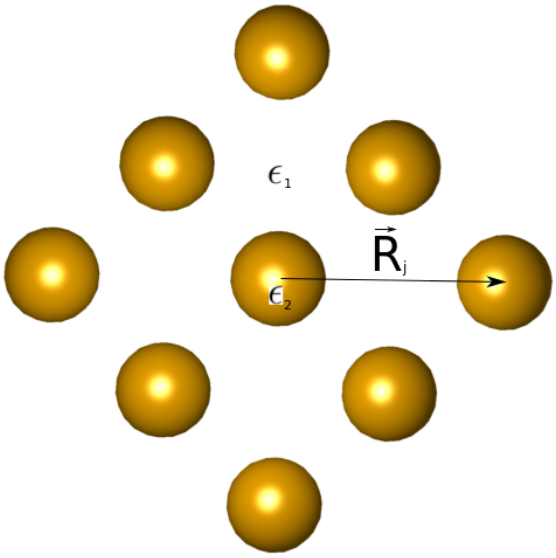

Figure 4.1.: 2D periodic array of identical nanospheres with periodic vector $\mathbf{R_i}$, all particles have the same dimensions and have the same ϵ_2, the environment has ϵ_1

With that in mind we can modify the equations for the potentials

$$\Phi(\mathbf{r}) = \int_{\partial\Omega_j} \Big(G_{j,0}(\mathbf{r}, \mathbf{r}')\sigma_{j,0}(\mathbf{r}') + \sum_{i \neq 0} G_{j,i}(\mathbf{r}, \mathbf{r}')\sigma_{j,i}(\mathbf{r}') \Big) da' + \Phi_{ext}(\mathbf{r}) \tag{4.2a}$$

$$\mathbf{A}(\mathbf{r}) = \int_{\partial\Omega_j} \Big(G_{j,0}(\mathbf{r}, \mathbf{r}')\, \mathbf{h}_{j,0}(\mathbf{r}') + \sum_{i \neq 0} G_{j,i}(\mathbf{r}, \mathbf{r}')\, \mathbf{h}_{j,i}(\mathbf{r}') \Big) da' + \mathbf{A}_{ext}(\mathbf{r}) \tag{4.2b}$$

where $G_{j,i}$ is the Green's function of the particle under consideration displaced by a

[2] 0 designates the "central" particle and i the surrounding periodic particles

periodic vector $\mathbf{R_i}$

$$G_{j,i}(\mathbf{r},\mathbf{r}') = \frac{e^{ik_j \mathfrak{r}_i}}{\mathfrak{r}_i} \quad , \quad \mathfrak{r}_i = |\,\mathbf{r}-\mathbf{r}'-\mathbf{R}_i\,| \tag{4.3}$$

The periodic vector will have the form of a 3-dimensional vector in the plane of the array

$$\mathbf{R}_i = \begin{pmatrix} x_i \cdot d \\ y_i \cdot d \\ 0 \end{pmatrix} \tag{4.4}$$

Here x_i and y_i are integers, and d is the distance between the particles.
With equations (4.2a) and (4.2b) we are able to calculate the potentials on the surface of one single particle (0) with the influence of the other particles (i) acting on the outer surface of that particle. It is important to recall at this point, that the effect of a source in medium 1 only excites the boundary on the side of medium 1 but not on the side of medium 2. Hence, in the following one only needs to consider the boundaries to medium $j = 1$.
The normal derivative is calculated straight forwardly

$$F_j = \mathbf{n}_j \cdot \nabla\Big(G_{j,0}(\mathbf{r},\mathbf{r}') + \sum_{i\neq 0} G_{j,i}(\mathbf{r},\mathbf{r}')\Big) \tag{4.5}$$

The consequences of these calculations are that the Green's functions propagate the electromagnetic effect of the other particles in the array to the one particle under consideration. The BEM can now be applied to solve for the surface charges and currents of one particle which are characterized by the influence of all other particles within the structure.

4.1.2. Phase factor

Last but not least, a phase factor has to be introduced to account for the incident angle of the incoming light excitation (plane wave excitation).
This is important due to the periodicity of the structure, because the phase factor is in general different for all particles of the array subject to the particle under consideration.

$$G_{j,0}(\mathbf{r},\mathbf{r}') + \sum_{i\neq 0} e^{i\,\mathbf{k}_j\,\mathbf{R}_i} G_{j,i}(\mathbf{r},\mathbf{r}'). \tag{4.6}$$

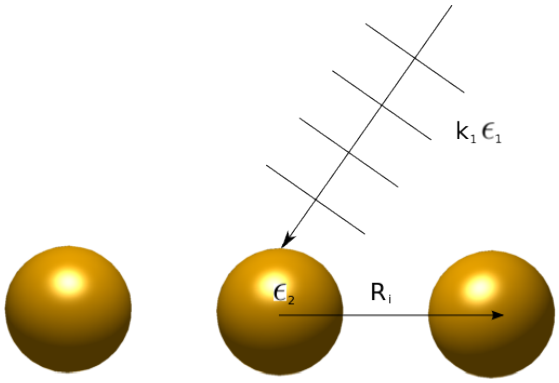

Figure 4.2.: plane wave excitation of the 2D periodic array.

Equation (4.6) gives the right phase factor as a function of the periodic vector $\mathbf{R}_i$ for each of the according Green's functions. In the above formula $k_j = k_1$, the wave vector of the incident light (inside medium 1).

4.1.3. Multipole expansion of the modified Green's function

In the previous sections it has been illustrated how to simulate the periodic structure utilizing the Green's functions. In this section another approximation will be introduced into the calculation of the potentials, the multipole expansion. The idea here is that for large enough distances to the particle under consideration, the Green's function can be approximated by a multipole expansion quite accurately.

$$G_j(\mathbf{r},\mathbf{r}') \rightarrow G_{j,0}(\mathbf{r},\mathbf{r}') + \sum_{i=-1}^{1} e^{i\,\mathbf{k}_j\,\mathbf{R}_i} G_{j,i}(\mathbf{r},\mathbf{r}') + \sum_{i\leq -2}^{\geq 2} G_{j,multi}(r,\Theta,\Phi) \tag{4.7}$$

The formula above states that the Green's function will be modified in a part for the particle under consideration $G_{j,0}$, a part for the next neighbors $G_{j,i}$ and for all particles further away than the next neighbors the multipole expansion of the Green's function $G_{j,multi}$ will be used.
The multipole expansion for the Green's function reads

$$G_{j,multi}(r,\Theta,\Phi) = ik_j \sum_{l=0}^{\infty} j_l(k_j r_<) h_l^{(1)}(k_j r_>) \sum_{m=-l}^{l} Y_{l,m}^*(\Theta',\Phi') Y_{l,m}(\Theta,\Phi) \tag{4.8}$$

Because this is an expansion in spherical coordinates the vector $\mathbf{r}$ will be converted into spherical coordinates $r_< = r$, Θ and Φ and the vector $\mathbf{r}' = \mathbf{r} + \mathbf{R}_i$ will be converted

into $r_> = r' + |R_i|$, Θ' and Φ'.
This again gives us the connection between two points in space $\mathbf{r}$ and $\mathbf{r}'$, which differ by a multiple of a periodic vector $\mathbf{R}_i$. The important part here is that we can hold on to the functions depending on $\mathbf{r}$ in every calculation because they design the "central" particle under consideration and do not change in all $G_{j,multi}$. The functions depending on $\mathbf{r}'$ represent the other particles in the array at all their positions in the periodic array. To compute the surface charges and currents we need to do the normal-derivation $F_{j,multi}(r, \Theta, \Phi)$ of the above expansion. For reasons of simplicity we follow the rule

$$F_{j,multi}(r, \Theta, \Phi) = \lim_{\epsilon \to \infty} \frac{G_{j,multi}(\mathbf{r} + \epsilon\, \hat{\mathbf{n}}, \mathbf{r}') - G_{j,multi}(\mathbf{r}, \mathbf{r}')}{\epsilon} \tag{4.9}$$

Where $\hat{\mathbf{n}}$ is the normal vector of the "central particle". By using equation (4.9) and (4.8) we first get

$$G_{j,multi}(r_n, \Theta_n, \Phi_n) = ik_j \sum_{l=0}^{\infty} j_l(k_j r_n) h_l^{(1)}(k_j r') \sum_{m=-l}^{l} Y_{l,m}^*(\Theta', \Phi') Y_{l,m}(\Theta_n, \Phi_n) \tag{4.10}$$

Here, $\mathbf{r} + \epsilon\, \hat{\mathbf{n}}$ has been converted into r_n, Θ_n and Φ_n. If we introduce this expression and equation (4.8) into (4.9), $F_{j,multi}(r, \Theta, \Phi)$ can be calculated. Hence, we are now able to solve BEM equations for the surface current $\mathbf{h}$.

4.2. Radiation of periodic structures

We have introduced the radiation fields of localized charge and current distributions in chapter 2. The subject of this chapter will be to use equation (2.40) for the calculation of the electric fields given by the surface currents which we have computed via the BEM.

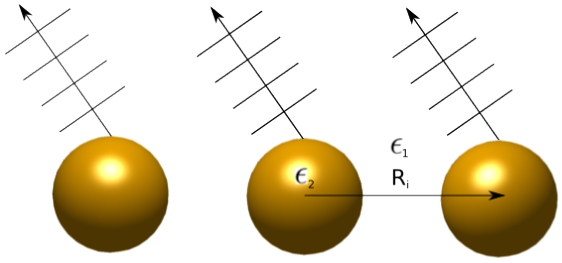

Figure 4.3.: Radiation from the periodic array.

In principle this is very easily done because we only have the current distribution of the "central" particle, and the periodic array is simulated through the Green's function that acts on said particle. But it is necessary to take the phase factors due to the periodicity into account

$$\mathbf{A}(\mathbf{r}) = \frac{e^{ikr}}{r} \int_V \sum_i \mathbf{h}_i(\mathbf{r}') e^{-ik\mathbf{n}(\mathbf{R}_i + \mathbf{r}')} e^{i\,\mathbf{k}\,\mathbf{R}_i} dV. \tag{4.11}$$

In this formula the first exponential accounts for the periodicity of the far field, meaning the outgoing waves of the radiation from the particle which behave like spherical waves due to $\frac{e^{ikr}}{r}$. The second exponential is due to the periodicity of the excitation light as in equation (4.6).

Now that we have the vector potential created by the surface current of the particle we can calculate the electric field from it. To do so one can make use of (2.5b)

$$\mathbf{E} = -\nabla\Phi + ik\,\mathbf{A}\,. \tag{4.12}$$

Because the contribution of $-\nabla\Phi$ produces only longitudinal components and the far field is transverse, we only take the contributions of $ik\,\mathbf{A}$ into account [12]. This results in

$$\tilde{\mathbf{E}}(\mathbf{r}) = ik \int_{\partial\Omega} \mathbf{h}_1(\mathbf{r}') \sum_i e^{-ik\mathbf{n}(\mathbf{R}_i + \mathbf{r}')} e^{i\,\mathbf{k}\,\mathbf{R}_i} da. \tag{4.13}$$

In the above formula we have rewritten the integral over a volume into a integral over a surface. In addition we used the fact that all particles in the considered array are identical and therefore each has the same surface current $\mathbf{h}_1$ which we can pull out of the sum.

Finally we need to make sure that all the contributions to the far field from equation (4.13) are transverse. To do so, we use the relation

$$\mathbf{E} = \tilde{\mathbf{E}} - (\tilde{\mathbf{E}} \cdot \mathbf{n})\mathbf{n}. \tag{4.14}$$

Hence, the induced electric field of a particle under influence of a periodic array reads

$$\mathbf{E}^{ind} \xrightarrow[kr\to\infty]{} \mathbf{E}\,\frac{e^{ikr}}{r}. \tag{4.15}$$

The time-averaged magnitude of the Poynting vector is

$$\langle S \rangle = \frac{\epsilon_0 c}{2} |\, \mathbf{E} \,|^2. \tag{4.16}$$

5. Simulation

5.1. MNPBEM

In the course of this thesis, in order to numerically calculate and simulate the surface charges and currents, as well as the electromagnetic fields, the Matlab toolbox MNPBEM has been used. The MNPBEM is a toolbox for the simulation of metallic nanoparticles (MNP) using the boundary element method (BEM), developed by Ulrich Hohenester and Andreas Trügler [1].
With this program it is possible to solve Maxwell's equations for a dielectric environment where the homogeneous and isotropic dielectric functions of the bodies in question, are separated by sharp interfaces. It is suited best for body sizes between a few to a few hundreds of nanometers, and for frequencies in the optical and near-infrared regime. A major advantage of the MNPBEM is that only the boundaries between the different dielectric materials have to be discretized instead of the whole volume, which results in overall faster simulations. In the previous chapters we have explained the theoretical foundation for the toolbox, whose operation method we will pictured in the following chapter.

5.1.1. Particle boundaries and dielectric environment

The simulation of the particle is done in two steps. To begin with, we need to define the dielectric functions ϵ_i for each medium i respectively[1]. Then we set up a function for the physical dimensions of the "geometrical" particle and discretize the particle boundaries for the system in question. This is done by chopping up the surface of the particle into small triangles (or squares), called faces. These discrete surface elements in figure 5.1 will be used to approximate the integrals in equations (2.35a) and (2.35b).

[1] ϵ can be a constant, a Drude dielectric function $\epsilon(\omega)$ or tabulated dielectric functions from experimental measurements

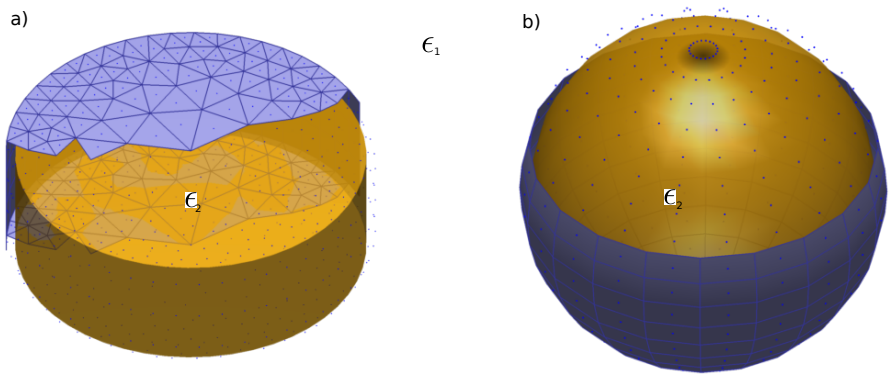

Figure 5.1.: a) surface discretization of a nanodisc with triangle faces and b) even surface discretization of a nanosphere with square faces, where the dots depicting the centroids of the vertices

When both is done, we can relate the particle boundary to the dielectric functions by defining the particle boundaries which are embedded in the dielectric environment. Through the surface normal $\hat{\mathbf{n}}$, whose direction is given by the order of the vertices of the face elements, we define the in- and outside of the boundary and assign a dielectric function to each of them.

5.1.2. BEM solvers

After the geometry and material properties have been set, we solve for the surface charges and currents with the BEM. This can be done with the quasistatic approximation of section 2.3.1 or the full Maxwell equations of section 2.3.2. For the excitation we use polarized plane waves in the optical spectrum[2].

To obtain a solution we have to compute the $N \times N$ matrices[3] of the respective BEM approach for the given wavelength. This calculation has to be conducted for every wavelength of interest. These calculations will be the most time-consuming part of the simulation. Runtimes depend on fineness of the discretization meaning the number of faces.

The excitation we choose will lead to the surface derivatives of the scalar potential for the quasistatic calculation and the scalar respectively vector potentials at the boundaries for the retarded case of the full Maxwell equations.

After running the program we arrive at the surface charges, currents and fields at the

[2]The excitation wave length is typically in the range between $\lambda_{exc} = 400\text{nm}$ - 700nm

[3]N is the number of faces used for the surface discretization

particle boundaries for the corresponding approach.
In conclusion we want to compare the quasistatic and the full (retarded) BEM solvers.

- The quasistatic solvers work best for structures significantly smaller than the light wavelength. Hence, dimensions of about a few tenth of nanometers to particles of the size $50nm$ to $100nm$, depending on the geometrical shape, should be used.

- The BEM simulation based on the full Maxwell equations are much slower than those of the quasistatic one. The reasons for this are the numerous matrix inversions seen in equations (2.37b), (2.38a) and (2.38b), because for a certain number of faces N, the time needed for a matrix inversion is of the order N^3.

In many cases it is indispensable to use the full Maxwell approach, like in ours. For our study of periodic structures only the full BEM solver is of use, because an array of nanoparticles is always greater than the effective scope of the quasistatic approach, therefore it is crucial to take retardation effects into account.

5.2. Spectra

5.2.1. Scattering and absorption cross section

From the surface charges, returned by the quasistatic BEM solvers, we can compute the scattering, absorption and extinction[4] cross section. These cross sections are calculated from the dipole moment induced on the particle boundaries. They are defined as

$$P_{sca} = \frac{8\pi}{3} k^4 |\mathbf{d}_\lambda|^2, \qquad P_{abs} = 4\pi k \Im(\hat{\mathbf{e}}_\lambda \cdot \mathbf{d}_\lambda),$$

where λ denotes the different polarizations $\hat{\mathbf{e}}$.
We can compute the cross sections in a very similar way for the full BEM solver, except that here the excitation also depends on the light propagation direction. the expressions for the cross sections are given by

$$P_{sca} = n_b \oint \Re\, \hat{\mathbf{n}} \cdot [\mathbf{E} \times \mathbf{B}]\, da, \qquad P_{ext} = -\frac{1}{n_b} \oint \Re\, \hat{\mathbf{n}} \cdot [\mathbf{E} \times \mathbf{B}^*_{inc} + \mathbf{E}^*_{inc} \times \mathbf{B}]\, da, \tag{5.1}$$

[4] extinction is the sum of scattering and absorption

with n_b being the refractive index of the embedding medium, $\mathbf{E}$, $\mathbf{B}$ are the scattered electromagnetic fields, and $\mathbf{E}_{inc}$, $\mathbf{B}_{inc}$ are the incoming electromagnetic fields of the planewave excitation.The integrand extends over a detector surface, usually a sphere at infinity.

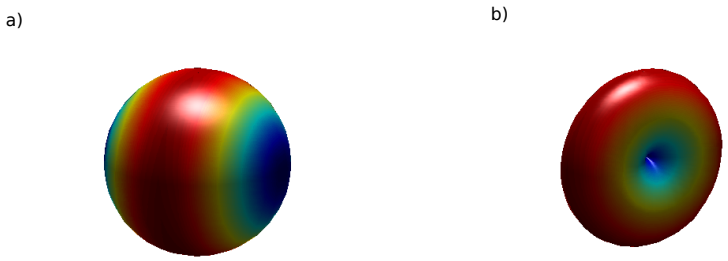

Figure 5.2.: a) surface charge distribution of a nanosphere (see figure 3.3) and b) dipole field of a nanosphere due to the charge oscillation excited by a planewave.

5.2.2. Extinction cross section with the optical theorem

We have mentioned above how to determine the extinction cross section through the sum of the scattering and absorption cross section, but there is another more elaborate way of calculation, through the optical theorem [13]. When considering a particle illuminated by a planewave polarized along the x-axis and propagating in $\hat{\mathbf{n}}_{inc}$ direction, we can expand this wave into counter-propagating spherical waves using Jones' lemma [14]. Therefore we, can obtain an expression for the extinction cross section C^{ext} of the particle (see A.8)

$$C^{ext} = \frac{4\pi}{k\mathcal{E}_0^{inc}} \Im \left[\hat{\mathbf{x}} \cdot \mathbf{E}_1^{sca}(\hat{\mathbf{n}}^{inc}) \right] . \tag{5.2}$$

Here, $\mathcal{E}^{inc}$ denotes the direction of the electric field, k is the wavenumber and $\hat{\mathbf{x}}$ is the polarization direction of the incident wave. This formula relates C^{ext} to the imaginary part of the scattering amplitude $\mathbf{E}_1^{sca}$ which is only evaluated in the direction of the incoming excitation $\hat{\mathbf{n}}^{inc}$.

5.3. Periodic structures with MNPBEM

In this section the program used to calculate the spectra of periodic structures will be outlined. The procedure can be divided into four steps:

- After a particle of arbitrary shape has been constructed with MNPBEM, the array needs to be simulated. This is done by taking the Green's function on the outside of the surface and, since we are dealing with an array of identical particles, use it to construct the outer surface Green's function for a particle in the structure by adding the periodic vector $\mathbf{R}_i$ like in equation (4.3), which denotes the position of the particle in the array. This way it is possible to simulate every particle in the structure through its outer Green's function which is sufficient to approximate the electromagnetic effect each particle has on the whole array.

- When the surface currents have been calculated with the BEM method, we need to compute the electric fields. To do so, we use equation (4.13) for the radiation in the far field, where we made the adjustment in the phase factor to account for the periodicity of the structure.

- For the next step, it is necessary to add a phase factor from equation (4.6) to the Green's functions and its normal derivative which accounts for the incident direction of the exciting light.

- As a last step, we make an approximation for particles in the array which are sufficiently far away from the "central" particle. Therefore we use the multipole expansion of equation (4.7) to approximate the Green's function of those particles. this should result in a decrease of computing time for big arrays with a sufficiently high discretization.

To conclude this section we should mention that the computing time in the simulation program greatly depends on the discretization N, which directly determines the size of the $N \times N$ Green's function matrices. Hence, the larger the matrices, the longer it will take to solve the BEM. Therefore, it will be essential to find the appropriate discretization for the according geometry of the particle, to minimize computing time and still get most accurate results for the surface currents and furthermore the spectra.

6. Results

In this section the simulation results of the periodic structures will be presented and discussed. For the gold nano particles we used an experimental dielectric function from [15]. To simplify the simulation we used a effective dielectric constant $\epsilon = 1.3$ for the embedding medium.
We will start by showing the spectra of periodic structures with two different particle geometeries. We will investigate a spherical-shaped particle, because it is very easy to calculate, and a disc-shaped particle because this geometry is widely used in experimental setups. We will see two important features, first how the increase in particle numbers or array size affect the spectra. Second, how different distances between the particles affect the spectra.
Then we will incorporate the angle dependence for the exciting light and show the effects of different incidence angles on the spectra.
In the finally section of this chapter, we will show how the multipole expansion can approximate the Green's functions and compare these results to the originals and we will outline the computing time needed for the calculation.

6.1. Spectra of periodic nanostructures

As mentioned above, for a single metal nanoparticle the resonance of the particle plasmon depends on the dielectric properties of the particle and its surrounding medium as well as its geometrical shape. For an ensemble of particles the plasmon resonance is additionally influenced by the electromagnetic particle interaction. These interactions are called near field coupling and far field interaction, respectively.
In the following we will only be concerned with far field interactions, because the array of nanoparticles that we are simulating has interparticle distances which exceed those capable of near field coupling. The far field interaction is mediated by scattered light fields of the nanostructure which are of dipolar nature. These dipolar fields interfere,

resulting in a collective radiation [16].
Furthermore, we use the retarded approach of section 2.3.2 in our simulation since the structure dimensions we are dealing with are square gratings of the size of $1200nm$ to $3600nm$, which are far greater than the wavelength of light so that the quasi static approach is no longer valid.
We start with a simple example, where we use the formula of section 4.1.1 to simulate a periodic array of spherical particles and look at the scattering cross section and the extinction cross section. For comparison, we then calculate the same cross sections for an array of nanodiscs, to visualize the importance of the particle geometries. We generate the sum of Green's functions in equation (4.1), by looping over all position of in the periodic structure. After that, we calculate the radiation of the particles. To do so, the following formulas of section 4.2 will be used. We use equation (4.13), where we have to calculate the phase factor for every constituent of the array, and then use equation (4.14) to get the correct transversal electric fields. The results are the combined far field spectra of the respective periodic arrays.

6.1.1. Dipolar interaction of nanoparticles

The plots in figure 6.1 show the scattering cross sections for arrays of metal nanospheres with a diameter of $60nm$ and discs with a diameter of $60nm$ and a hight of $20nm$. The scattering cross section is plotted as a function of the wavelength and grating constant ranging from $300nm$ to $1300nm$. The light excitation is polarized in the direction of the array and its angle of incident is $\pi/2$, meaning the excitation source is located $90°$ above the array.

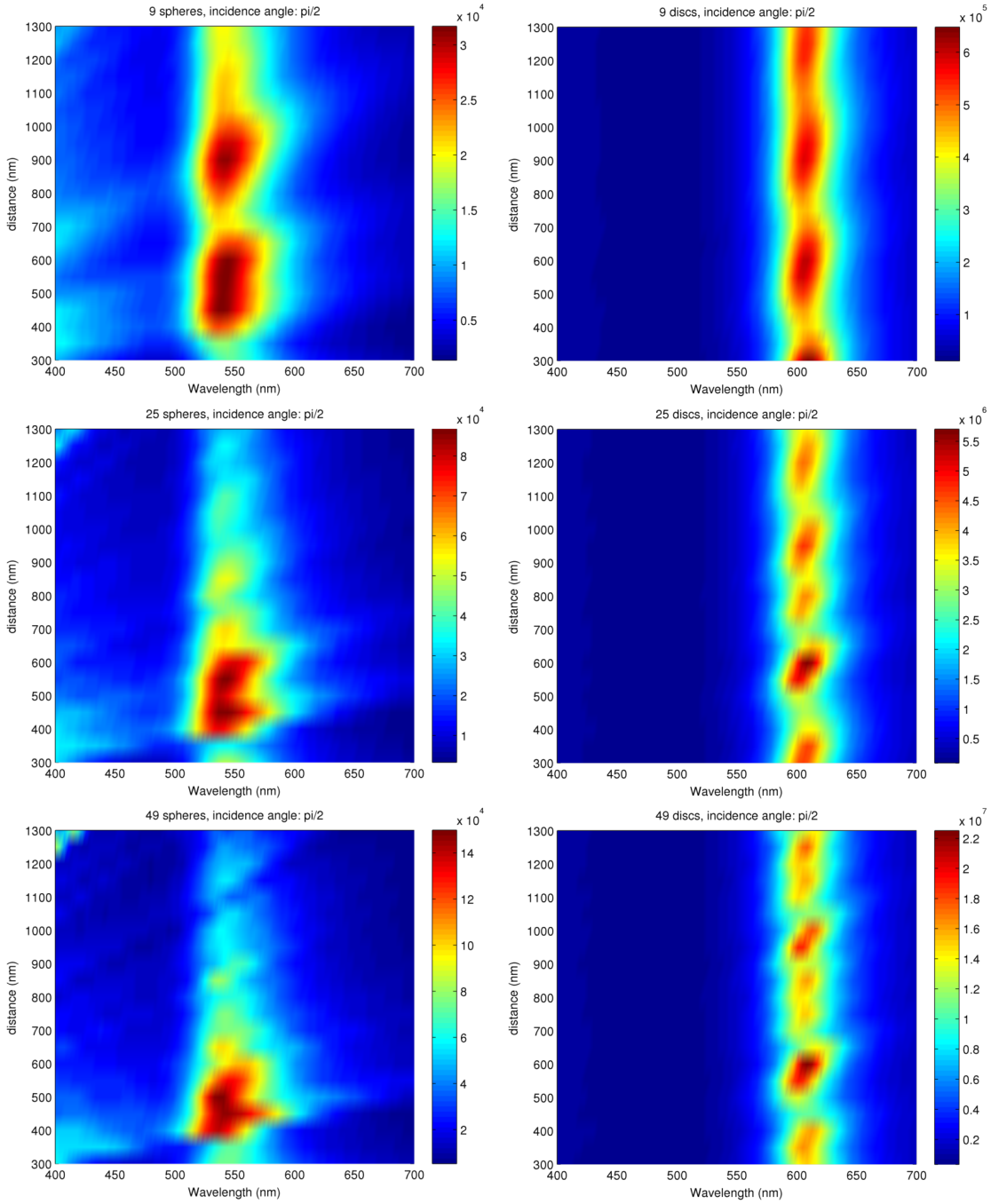

Figure 6.1.: The scattering cross sections of arrays with 9, 25 and 49 particles. The six plots show the cross sections for distances between particles of $300nm$ to $1300nm$, for spheres on the left and discs on the right side respectively.

For two dimensional square gratings of metal nanoparticles particularly strong dipolar interaction arise at specific grating orders. In figure 6.1, we see the grating orders where the constructive interference of the scattered light fields occur. The strength of these grating orders depend on the number of particles in the structure. Array sizes of 9, 25 and 49 particles have been simulated and it can be seen that the peaks become higher and more localized as a function of the array size at the resonance wavelengths for the respective particles. The resonance wavelength is also smeared over a range of about $40nm$. This happens when the scattered light fields change from evanescent to radiating character [17]. For distances smaller than this grating orders the fields are evanescent but the local fields are quite large in the array plane. Due to this effect, the plasmon resonance is modified which results in a redshift of resonance wavelength as can be seen in figure 6.1.

6.1.2. Extinction spectra

In figure 6.2, we can see that the extinction cross section is narrowing when the array size is increased, which means a higher and sharper peak at the resonance wavelength of the particles and therefore a shorter lifetime of the particles plasmons. Another noteworthy point is the dependence of the extinction on the particle size due to retardation effects.

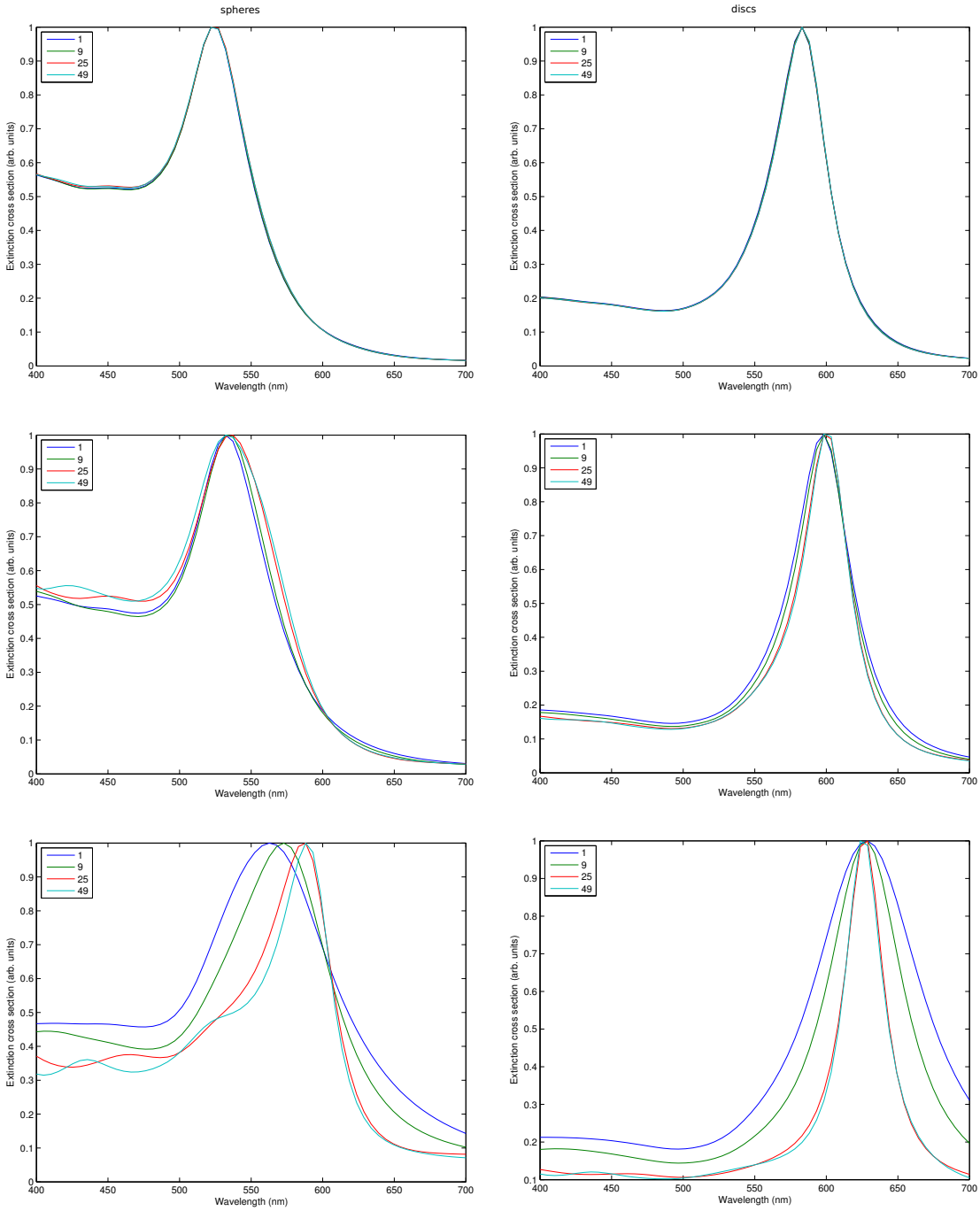

Figure 6.2.: Normalized extinction cross section for different particles sizes and array sizes. The distance of the particles in the array is kept constant at $600nm$ in each plot. The left plots show the extinction for spheres with diameters of $30nm$, $60nm$ and $100nm$. The right plots show discs with diameters of $30nm$, $60nm$ and $100nm$ and heights of $10nm$, $20nm$ and $40nm$.

In figure 6.3 we display how the electromagnetic fields of the particles in the array are shaped for different numbers of golden nanospheres respectively.

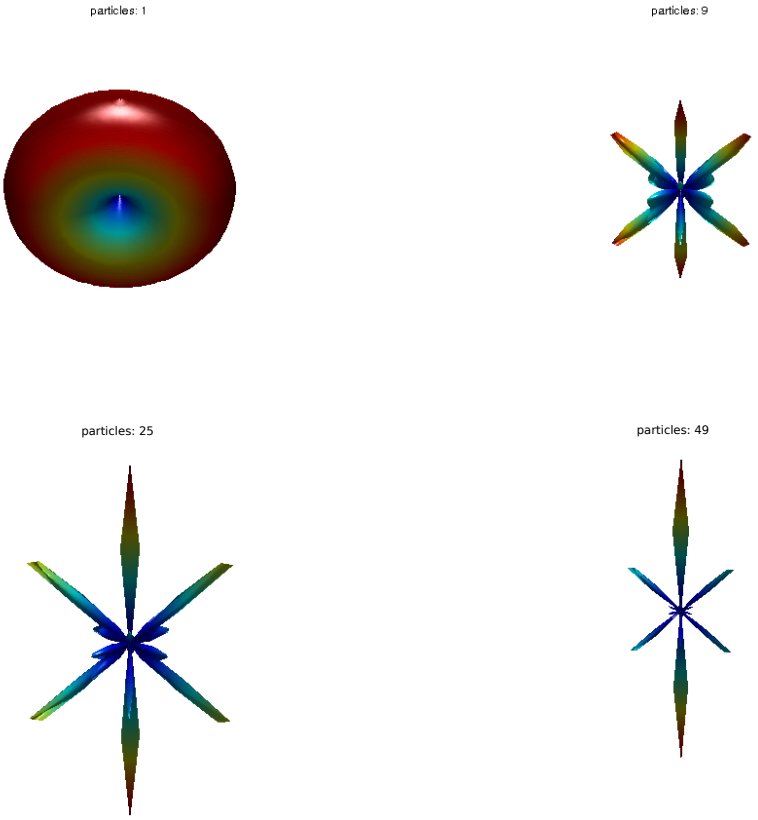

Figure 6.3.: These plots show the differential scattering cross section, for particles with diameter of $60nm$ and distances of $600nm$. We can see how a single particles emits a essential dipole field and that the fields get deformed with increasing array size, because the dipolar fields interfere to a collective radiation, and depending on the inter particles distances the interference is more constructive or more destructive.

It shows the far field of the array. One particle emits a dipolar field, but in a periodic array the particle plasmons interact with each other collectively, which results in fields that are of higher intensity and much more focused in space.

6.1.3. Angle dependence

In this section we incorporate equation (4.6) into the calculation we used in previous section. Thus, we can account for the incident angle of the excitation which changes the spectra. Because of the array structure we need to add the phase term to the Green's functions in equation (4.1) as well as the phase factor in the calculation of the electric fields equation (4.13).
Due to the different incidence angles the positions of the maxima change as shown in figure 6.4 for an incidence angle of $\pi/3$, figure 6.5 for $\pi/4$ and figure 6.6 for $\pi/6$. Because of the incident angle the particles in the array are no more illuminated with the same phase. Due to this, the effective distances between the particles change and so dose the constructive interference hence, the grating orders of the peak wavelengths change.
It can be seen that the scattering cross section is strongly angle dependent, especially for the discs. The peak hight increases with increasing array size but the positions of the grating orders do not change.

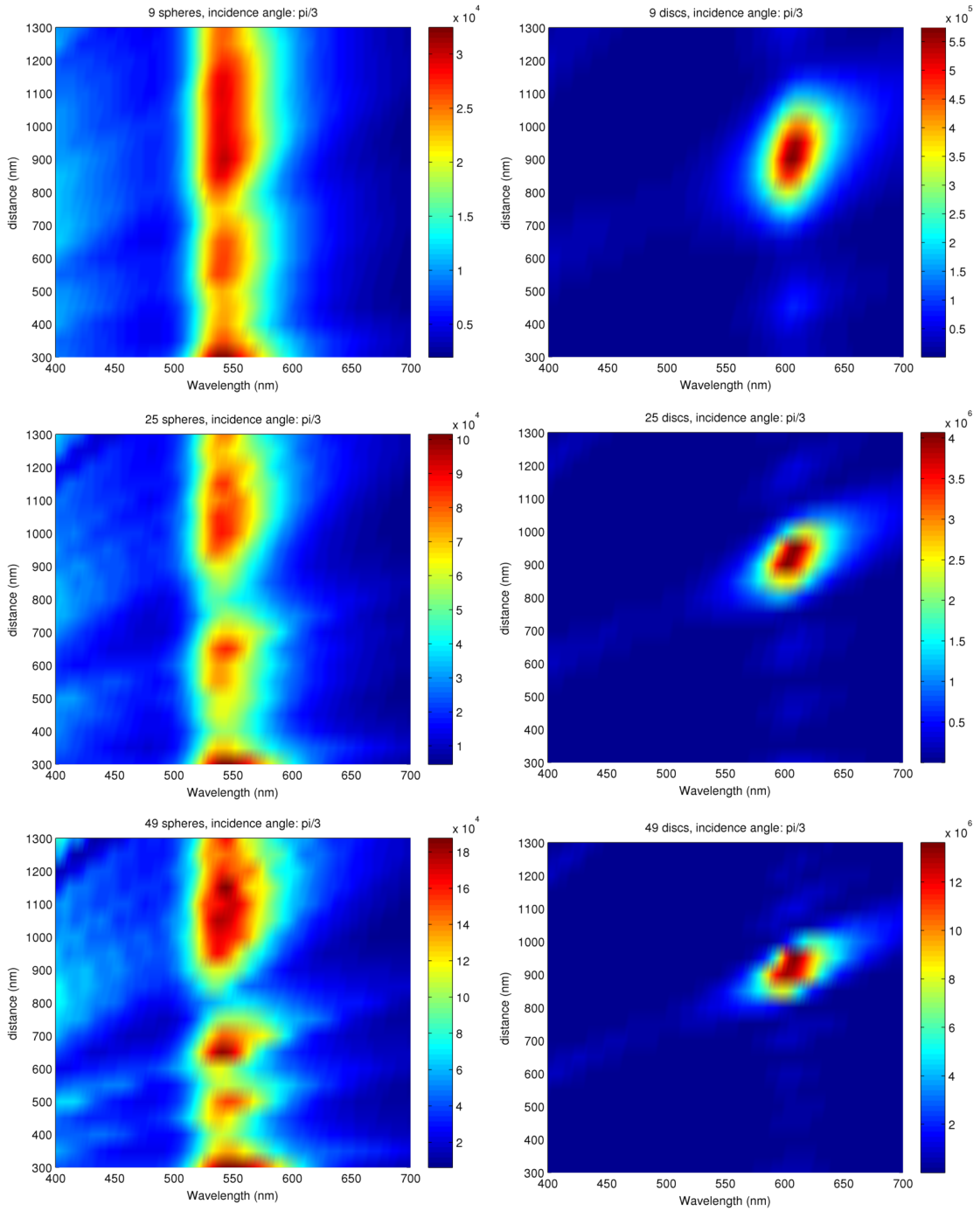

Figure 6.4.: The scattering cross section for spherical particles and discs as a function of the distance with a 60° incident angles of the light excitation.

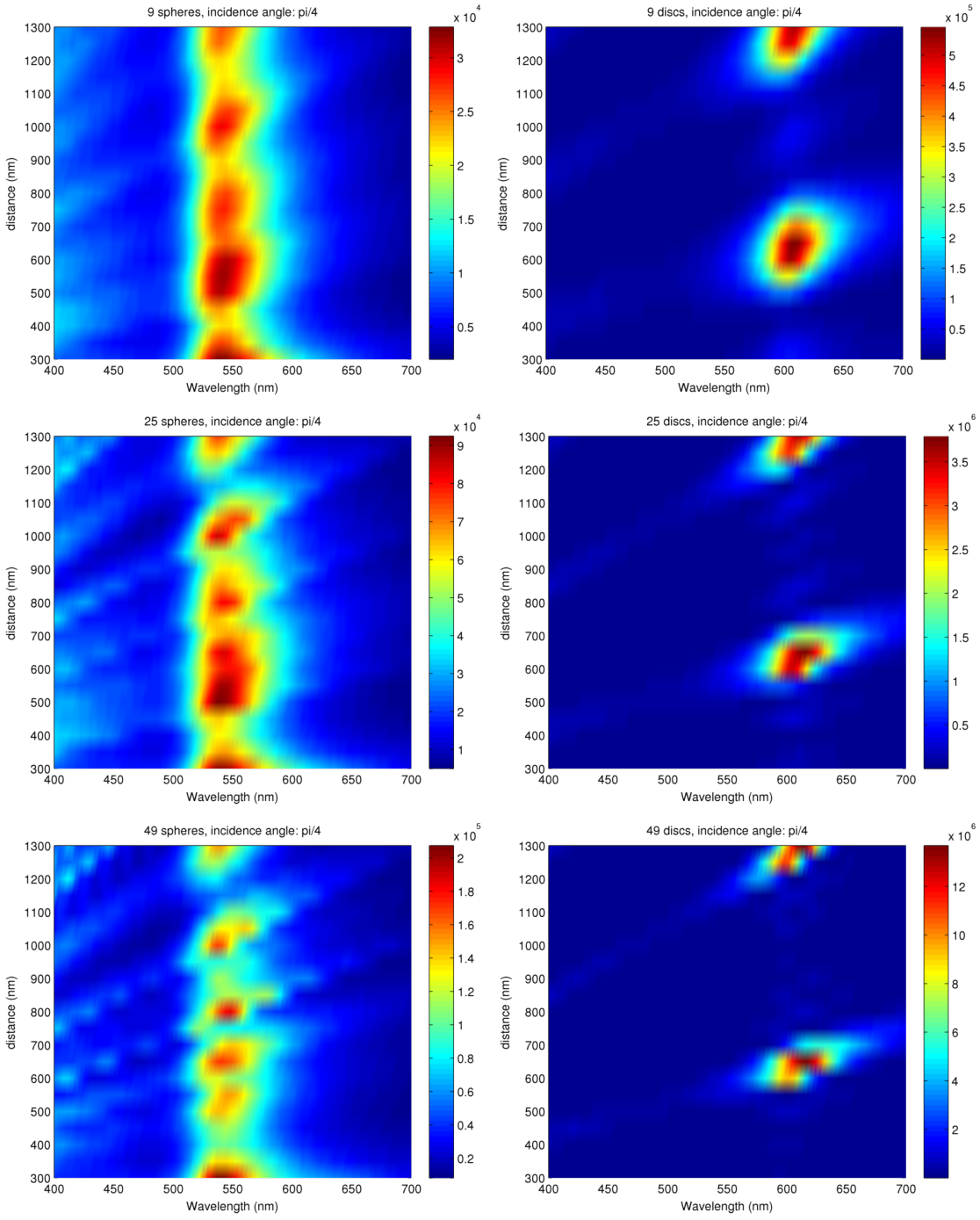

Figure 6.5.: The scattering cross section for spherical particles and discs as a function of the distance with a $45°$ incident angles of the light excitation.

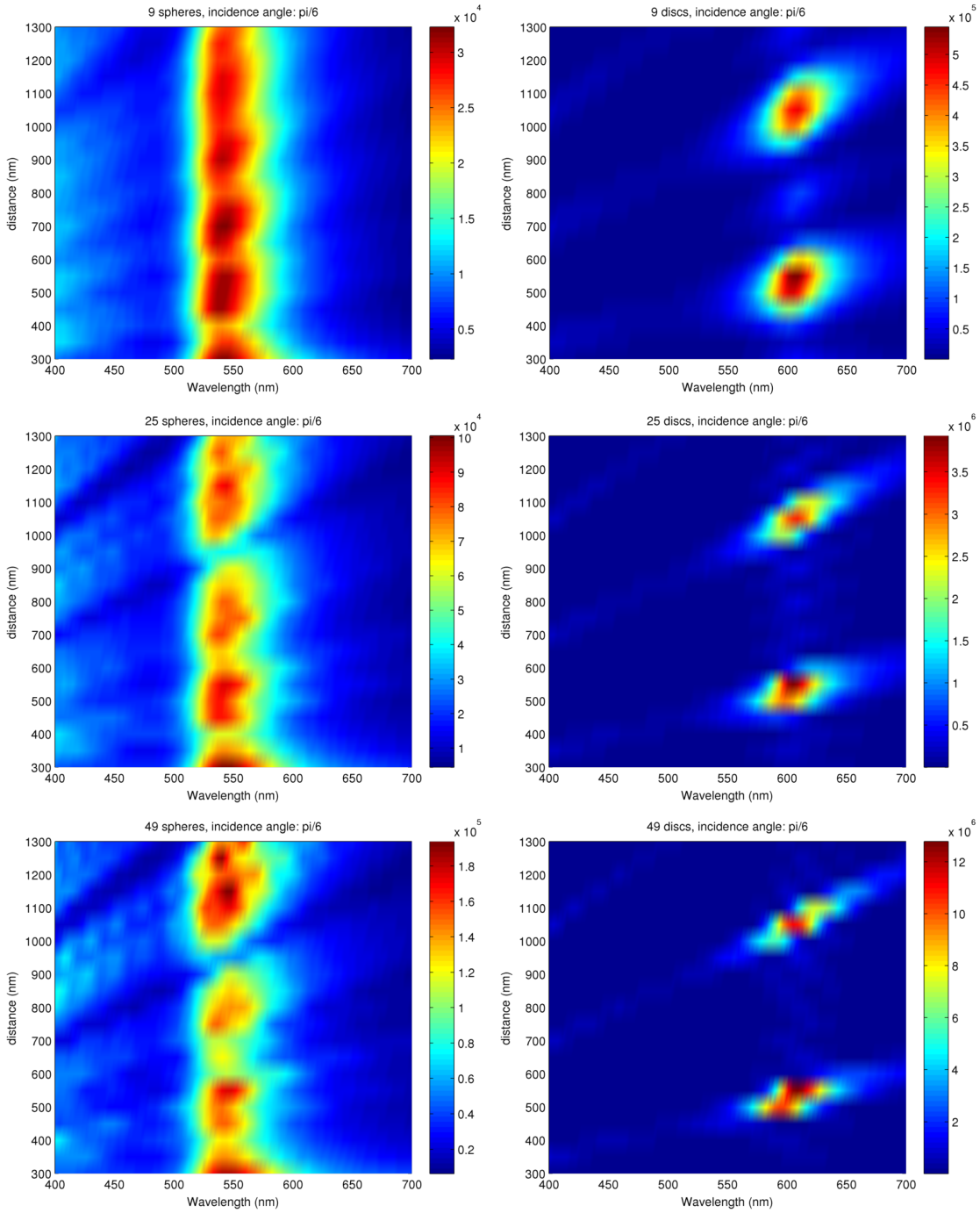

Figure 6.6.: The scattering cross section for spherical particles and discs as a function of the distance with a 30° incident angles of the light excitation.

6.2. Multipole expansion

This section will deal with the multipole expansion of the Green's function as given in section 4.1.3. First we will discuss how the expansion of equation (4.8) can be implemented into equation (4.7) and under which circumstances it is valid.
As a second step the matter of computing times and efficiency shall be briefly discussed. Only some estimations will be given since the actual computing times depend on the precise implementation in the MNPBEM which has not been conducted yet.

6.2.1. Comparison of the Green's function with the multipole expansion

The formal approach for the multipole expansion has been given in equation (4.8) but the question is how to utilize this in the MNPBEM toolbox.
In this Toolbox the positions of surface elements is expanded, by the means of a mesh grid, into a matrix which will be used to compute the Green's functions and its normal derivatives. This matrix approach is key to all the calculations conducted in MNPBEM. But the multipole expansion of section 4.1.3 incorporates just the position of the surface elements, because otherwise we would not gain any advantages out of it. So to make the multipole expansion into a matrix as well we rewrite equation (4.8) like

$$G_{j,milti}(r,\Theta,\Phi) = ik \sum_{l,m} \underbrace{j_l(k_j r) * Y_{l,m}(\Theta,\Phi)}_{U_{l,ml}(r,\Theta,\Phi)} * \underbrace{h_l(k_j r') * Y^*_{l,m}(\Theta',\Phi')}_{V_{l,m}(r',\Theta',\Phi')}.$$

Here, the multipole expansion has been separated into a part only depending of r which represents the "central particle" and a part depending on r' which denotes all the other particles in the array we want to simulate. With this separation we can now write

$$\frac{e^{(ik|r-r'|)}}{4\pi|r-r'|} = ik \sum_{l,m} U_{l,m}(r,\Theta,\Phi) * V^T_{l,m}(r',\Theta',\Phi'),$$

which now has matrix form and the same size and composition as the Green's function. A similar procedure has to be done for $F_{j,multi}$, the normal derivative of $G_{j,multi}$, where we use equation (4.10) and arrive at

$$G_{j,multi}(\mathbf{r}+\epsilon\,\hat{\mathbf{n}},\mathbf{r}') = ik\sum_{l,m} U_{l,m}(r_n,\Theta_n,\Phi_n) * V^T_{l,m}(r',\Theta',\Phi'),$$

which leads us to $F_{j,multi}$. A noteworthy point here is that only $U_{l,m}$ has to be modified for the normal derivative and $V^T_{l,m}$ stays the same.
As can easily be seen, the quality of the multipole expansion depends on its order l. In the following we will depict that and the dependence of the distance to the other particles in the structure. This can be done by calculating the difference between the Multipole Expansion and the Green's function and norm the result, like $\frac{|G_{j,multi}(r,\Theta,\Phi)-G_j(\mathbf{r},\mathbf{r}')|}{|G_j(\mathbf{r},\mathbf{r}')|}$.

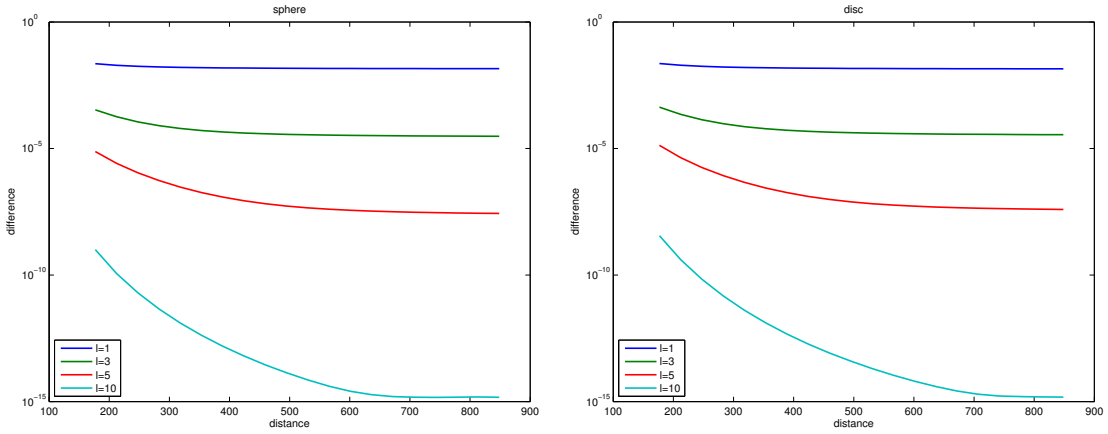

Figure 6.7.: This figure shows the behavior of the difference between G_{multi} and G as a function of the particle distance for different orders of the multipole expansion. The error of the expanded Green's function becomes very small with higher orders of l. Important is that the error becomes smaller with increasing distance form the "central" particle. This is in agreement with the used approach, simulating the next neighbors with G and all other particles through G_{multi}.

6.2.2. Computing time and efficiency

As mentioned before there are several ways to calculate a periodic nano structure in the framework of the MNPBEM. In this section we will discuss the advantages of the approaches elaborated in the chapters above.

The first and most direct approach would be the explicit simulation of all particles at the respective positions with the MNPBEM. This would be the most time consuming way

because the calculation of the Green's function and its inverse, depending on the size of those matrices, take the most time to compute. As mentioned above the computing time goes like N^3 with N being the number of surface elements and they must be executed for each of the n particles in the structure.

If we use the approach of section 4.1.1 we only would have to calculate one "central" particle completely. The remaining particles surrounding the one under consideration are only incorporated trough a loop over the surface Green's function in the array and calculation of these periodic Green's functions, their normal derivative, and the phase factors, is now the main concern. This loop is dependent on the number of particles and the process will become more costly in terms of time with increase of the array size, but it is significantly faster than the calculation of each particle. It is also necessary to point out that with higher numbers of particles in the array the far field radiation becomes more focused. In order to calculate them correctly the discretization has to be increased with the number of particles which in turn increases the size of the matrices.

To increase the efficiency of the computational procedure further we use the multipole expansion of the Green's function to simulate particles beyond the next neighbors. As seen in the previous section, at a certain distance the difference between the regular Green's function and its multipole expansion is small enough to justify the replacement. The advantage is that the multipole expansion dose not calculate matrices but vectors with length $N \times 3$ instead, and only afterwards the matrices are created through $U_{l,m} * V_{l,m}^T$. The computing time of course depends on the number of orders l of the expansion we wish to take into account but with higher discretization, which is need as mentioned before, and increasing size of the structure the multipole expansion becomes more favorable.

In table 6.1 we compare the computing time of the three approaches and for different array sizes and discretization. Since the functions used in this thesis are not yet implemented in the MNPBEM toolbox, the computing times given in the table may not be absolutely accurate but it shows the ratio. Another influence on the computing time is the amount of working memory available and possible parallelizations of the program.

[1] number of surface elements on each particle

approach:	# of particles	discretization[1]	time(sec)
direct calculation	1	1200	300
	1	1600	650
	9	1200	2700
	9	1600	5500
periodic function	9	1200	350
	9	1600	780
	25	1200	520
	25	1600	1000
	25	2000	1700
	49	1200	770
	49	1600	1400
	49	2000	2400
multipole expansion	25	1200	470
	25	1600	960
	25	2000	1600
	49	1200	680
	49	1600	1200
	49	2000	2100

Table 6.1.: This table shows the computing time for the different approaches depending on the number of particles and the discretization. It can be seen that the direct calculation through simulation of all the particles in the array separately is very time consuming. The calculation through the periodic Green's function is a good step forward in terms of computing time. The multipole expansion becomes more important if the number of particles and the discretization becomes larger than 9 particles.

7. Acknowledgements

First of all I want to thank my family and especially my parents Franz and Christine for their patients and support in the last years, and who inspired me to study in Graz in the first place.

I also want to thank Univ. Prof. Ulrich Hohenester for the guidance and advice he provided during the creation of this thesis.

Special thanks goes to Mag. Jürgen Waxenegger who was a great help throughout this howl time. The discussions with him were always most fruitful and entertaining. Another special thanks goes to Mag. Anton Hörl who inspired the theoretical part of this thesis and was a great colleague.

Finally I want to thank all my friends and other colleagues during the time at the university of Graz, who made it memorable and fun.

A. Appendix

A.1. Time harmonic fields

The spectrum $\hat{\mathbf{E}}(\mathbf{r},\omega)$ of a time-dependent field $\mathbf{E}(\mathbf{r},\omega)$ is defined by the Fourier transform [6]

$$\hat{\mathbf{E}}(\mathbf{r},\omega) = \frac{1}{2\pi}\int_{-\infty}^{\infty} \mathbf{E}(\mathbf{r},t)e^{i\omega t}dt \tag{A.1}$$

We need $\mathbf{E}(\mathbf{r},\omega)$ to be real so

$$\hat{\mathbf{E}}(\mathbf{r},-\omega) = \hat{\mathbf{E}}^{*}(\mathbf{r},\omega) \tag{A.2}$$

Now we apply the Fourier transform (A.1) to the Maxwell equations (2.1a-d) and get

$$\nabla \times \hat{\mathbf{E}}(\mathbf{r},\omega) = i\omega\hat{\mathbf{B}}(\mathbf{r},\omega) \tag{A.3a}$$
$$\nabla \times \hat{\mathbf{H}}(\mathbf{r},\omega) = -i\omega\hat{\mathbf{D}}(\mathbf{r},\omega) + \hat{\mathbf{j}}(\mathbf{r},\omega) \tag{A.3b}$$
$$\nabla \cdot \hat{D}(\mathbf{r},\omega) = \hat{\rho}(\mathbf{r},\omega) \tag{A.3c}$$
$$\nabla \cdot \hat{\mathbf{B}}(\mathbf{r},\omega) = 0 \tag{A.3d}$$

With the solution for $\hat{\mathbf{E}}$ the time-dependent field can be calculated by inverse transform

$$\mathbf{E}(\mathbf{r},t) = \int_{-\infty}^{\infty} \hat{\mathbf{E}}(\mathbf{r},\omega)e^{i\omega t}dt \tag{A.4}$$

Thus, through transformation every spectral component can be treated as a separated monochromatic field. The time dependence can be obtained by the inverse transformation.

For time-harmonic fields, the time dependence in the wave equation can be separated

to yield a harmonic differential equation. A monochromatic field can now be written as

$$\mathbf{E}(\mathbf{r},t) = \Re\left[\mathbf{E}(\mathbf{r})e^{-i\omega t}\right] = \frac{1}{2}\left[\mathbf{E}(\mathbf{r})e^{-i\omega t} + \mathbf{E}^*(\mathbf{r})e^{i\omega t}\right], \tag{A.5}$$

with similar expressions for other fields.

A.2. Derivation of the Helmholtz equations

One can take the curl on Ampére's law (2.3b) in frequence space [6], which gives

$$\nabla \times \nabla \times \mathbf{E}(\mathbf{r},\omega) = \nabla \times i\frac{\omega}{c}\mathbf{B}(\mathbf{r},\omega). \tag{A.6}$$

The left-hand side reduces to

$$\nabla \times \nabla \times \mathbf{E}(\mathbf{r},\omega) = \nabla(\nabla \cdot \mathbf{E}(\mathbf{r},\omega)) - (\nabla \cdot \nabla)\,\mathbf{E}(\mathbf{r},\omega) = \nabla^2\,\mathbf{E}(\mathbf{r},\omega), \tag{A.7}$$

and the right-hand side becomes

$$\nabla \times i\frac{\omega}{c}\,\mathbf{B}(\mathbf{r},\omega) = i\frac{\omega}{c}(i\frac{\omega}{c}\,\mathbf{D}(\mathbf{r},\omega)) = \frac{\omega^2}{c^2}\epsilon\,\mathbf{E}(\mathbf{r},\omega) = \epsilon k^2\,\mathbf{E}(\mathbf{r},\omega). \tag{A.8}$$

A similar expression holds for Faraday's law (2.3b) . This leads to second order partial differential equations, called the Helmholz equations

$$(\nabla^2 + \epsilon k^2)\,\mathbf{E}(\mathbf{r},\omega) = 0, \tag{A.9a}$$

$$(\nabla^2 + \epsilon k^2)\,\mathbf{B}(\mathbf{r},\omega) = 0. \tag{A.9b}$$

A.3. Derivation of the Green's function

To obtain the solution to the scalar wave equation [18]

$$(\nabla^2 + k^2)\Psi(\mathbf{r}) = s(\mathbf{r}), \tag{A.10}$$

in some volume V, with the source term $s(r)$, we first need to determine the Green's function in the same volume V. That function is the solution to the following equation

$$(\nabla^2 + k^2)g(\mathbf{r},\mathbf{r}') = \delta(\mathbf{r}-\mathbf{r}'). \tag{A.11}$$

The functions $g(\mathbf{r}, \mathbf{r}')$ and $\Psi(\mathbf{r})$ can be found, due to the principle of linear superposition, since $g(\mathbf{r}, \mathbf{r}')$ is the solution of (A.10) with a point source on the right-hand side. This can be seen from

$$s(\mathbf{r}) = \int d\,\mathbf{r}'\, s(\mathbf{r}')\delta(\mathbf{r} - \mathbf{r}'), \tag{A.12}$$

which is a linear superposition of the point sources. Therefore the solution of (A.10) is

$$\Psi(\mathbf{r}) = -\int_V d\,\mathbf{r}'\, g(\mathbf{r}, \mathbf{r}')s(\mathbf{r}'), \tag{A.13}$$

which is an integral linear superposition of the solution of (A.11). Further, it can be seen that $g(\mathbf{r}, \mathbf{r}') = g(\mathbf{r}', \mathbf{r})$ from the shape of V. To find the solution of equation (A.11) for an unbounded, homogeneous medium, one has to solve it in spherical coordinates with the origin at $\mathbf{r}'$. So (A.11) becomes

$$(\nabla^2 + k^2)g(\mathbf{r}) = \delta(\mathbf{r}) = -\delta(x)\delta(y)\delta(z). \tag{A.14}$$

Due to the spherical symmetry of a point source , $g(\mathbf{r})$ must have the same symmetry. Then for $r \neq 0$, the homogeneous, spherically symmetric solution to (A.14) is given by

$$g(\mathbf{r}) = C\frac{e^{ikr}}{r} + D\frac{e^{-ikr}}{r}. \tag{A.15}$$

Because physical grounds imply that there are no sources at infinity, only the outgoing solution

$$g(\mathbf{r}) = C\frac{e^{ikr}}{r}, \tag{A.16}$$

of (A.15) can exist. The constant C can be found by matching the singularities at the origin on both sides of equation (A.14). To do so, one substitutes (A.16) into (A.14) and integrates over a small volume around the origin to get

$$\int_{\Delta V} dV \nabla \cdot \nabla C\frac{e^{ikr}}{r} + \int_{\Delta V} dV k^2 C\frac{e^{ikr}}{r} = -1. \tag{A.17}$$

The second integral vanishes when $\Delta V \to 0$, because $dV = 4\pi r^2 dr$. By using Gauss' theorem, the first integral in equation (A.17) can be converted into a surface integral, which yields

$$\lim_{r\to 0} 4\pi r^2 \frac{d}{dr} C\frac{e^{ikr}}{r} = -1, \tag{A.18}$$

or $C = 1/4\pi$. The solution to (A.11) must depend on $|\,\mathbf{r}-\mathbf{r}'\,|$ only. Therefore, in general,

$$g(\mathbf{r},\mathbf{r}') = g(\mathbf{r}-\mathbf{r}') = \frac{e^{ik|\,\mathbf{r}-\mathbf{r}\,|}}{|\,\mathbf{r}-\mathbf{r}'\,|}, \tag{A.19}$$

which implies that $g(\mathbf{r},\mathbf{r}')$ is translational invariant for unbounded, homogeneous media. Hence, the solution to equation (A.10), from (A.13), then is

$$\Psi(\mathbf{r}) = -\int_V d\,\mathbf{r}'\,\frac{e^{ik|\,\mathbf{r}-\mathbf{r}\,|}}{|\,\mathbf{r}-\mathbf{r}'\,|}s(\mathbf{r}'). \tag{A.20}$$

A.4. Electromagnetic boundary conditions

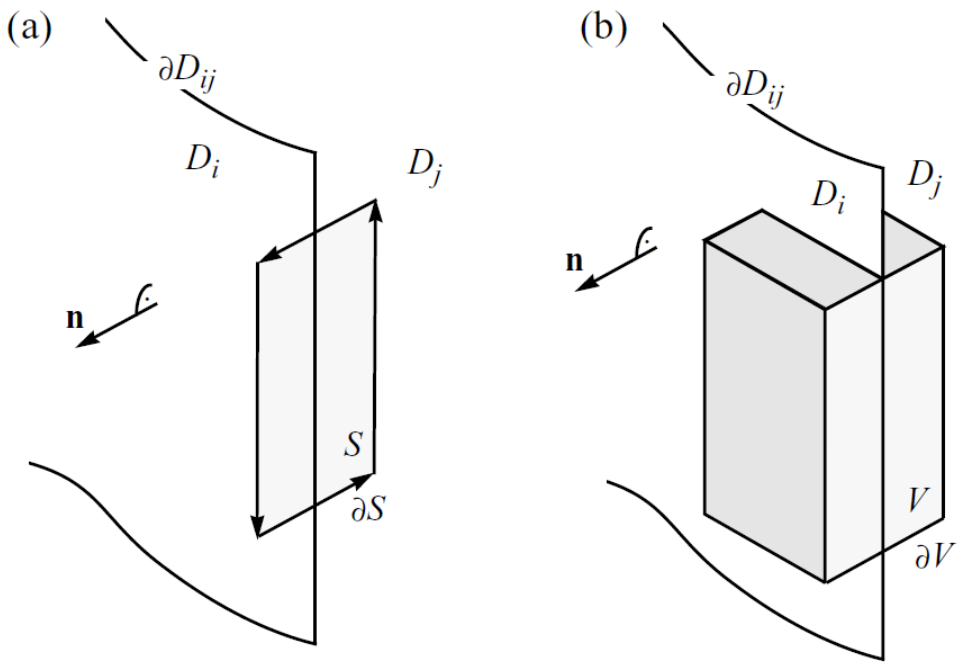

Figure A.1.: Integration paths for the derivation of the boundary conditions on the interface ∂D_{ij} between two adjacent domains D_i and D_j [6].

In order to derive the boundary conditions for two media we write Maxwell's equations

(2.1a) and (2.1b) in their integral form[1]

$$\oint_{\partial V} \mathbf{D} \cdot \hat{\mathbf{n}}\, da = 4\pi \int_V \rho(\mathbf{r}, t) dV, \tag{A.21a}$$

$$\oint_{\partial V} \mathbf{B} \cdot \hat{\mathbf{n}}\, da = 0. \tag{A.21b}$$

If the volume element V, in figure A.1, is infinitesimal small the equations (A.21a) and (A.21b) become

$$\oint_{\partial V} \mathbf{D} \cdot \hat{\mathbf{n}}\, da = (\mathbf{D}_i - \mathbf{D}_j) \cdot \hat{\mathbf{n}}\, \Delta a,$$

$$\oint_{\partial V} \mathbf{B} \cdot \hat{\mathbf{n}}\, da = (\mathbf{B}_i - \mathbf{B}_j) \cdot \hat{\mathbf{n}}\, \Delta da.$$

The right-hand side of (A.21a) takes the form

$$4\pi \int_V \rho dV = 4\pi\sigma\Delta a.$$

Therefore, the normal components of $\mathbf{D}$ and $\mathbf{B}$ are

$$(\mathbf{D}_i - \mathbf{D}_j) \cdot \hat{\mathbf{n}} = 4\pi\sigma, \tag{A.23a}$$

$$(\mathbf{B}_i - \mathbf{B}_j) \cdot \hat{\mathbf{n}} = 0, \tag{A.23b}$$

meaning that the normal component of $\mathbf{B}$ is continuous at the interface and the normal component of $\mathbf{D}$ is discontinuous and equal to the surface charge density σ at the interface enclosed by V.

In order to find the tangential boundary conditions, we evaluate the integral form of

[1] in the following we omit the arguments $(\mathbf{r}, t)$ of the fields

(2.1c) and (2.1d) for the infinitesimal contour S

$$\oint_{\partial S} \mathbf{H} \cdot ds = \frac{1}{c} \int_S 4\pi \, \mathbf{j} + \frac{\partial \mathbf{D}}{\partial t} \cdot \hat{\mathbf{n}} \, da, \tag{A.24a}$$

$$\oint_{\partial S} \mathbf{E} \cdot ds = -\frac{1}{c} \int_S \frac{\partial \mathbf{B}}{\partial t} \cdot \hat{\mathbf{n}} \, da, \tag{A.24b}$$

which leads to

$$\hat{\mathbf{n}} \times (\mathbf{E}_i - \mathbf{E}_j) = 0, \tag{A.25a}$$

$$\hat{\mathbf{n}} \times (\mathbf{H}_i - \mathbf{H}_j) = \mathbf{j} \, . \tag{A.25b}$$

Hence, the tangential component of $\mathbf{E}$ is continuous at the interface and the tangential component of $\mathbf{H}$ is discontinuous, with the discontinuity at the interface being the surface current density $\mathbf{j}$.

A.5. Boundary conditions for potentials

In the quasi static regime equation (A.23a) can be written as

$$(\epsilon_1 \nabla \Phi_1 - \epsilon_2 \nabla \Phi_2) = 0,$$

or equally we get for the normal components of the potential

$$\epsilon_1 \frac{\partial \Phi_1}{\partial n} = \epsilon_2 \frac{\partial \Phi_2}{\partial n}, \tag{A.26}$$

with

$$\epsilon_i \frac{\partial \Phi_i}{\partial n} = \hat{\mathbf{n}} \cdot \nabla \Phi_i,$$

being the surface derivative of the potential at a certain point of the interface. For the tangential components we get

$$(\nabla \Phi_1)^{||} = (\nabla \Phi_2)^{||}. \tag{A.27}$$

A.6. Full Maxwell equations

The continuity of the tangential magnetic field reads [9]

$$\mathbf{H}_1\,\mathbf{h}_1 - \mathbf{H}_2\,\mathbf{h}_2 - ik\,\hat{\mathbf{n}}(G_1\epsilon_1\sigma_1 - G_2\epsilon_2\sigma_2) = \Delta\,\mathbf{A}'_{ext} + ik\,\hat{\mathbf{n}}(\epsilon_1\Phi_1 - \epsilon_2\Phi_2), \tag{A.28}$$

with $H_{1,2} = F \pm 2\pi\mathbb{1}$.

The continuity of the normal electric field displacement gives

$$\begin{aligned}\mathbf{H}_1\,\epsilon_1\sigma_1 - \mathbf{H}_2\,\epsilon_2\sigma_2 - ik\,\hat{\mathbf{n}}\cdot(G_1\epsilon_1\,\mathbf{h}_1 - G_2\epsilon_2\,\mathbf{h}_2) = \\ \epsilon_1(ik\,\hat{\mathbf{n}}\cdot\mathbf{A}_1^{ext} - \Phi'_1) - \epsilon_2(ik\,\hat{\mathbf{n}}\cdot\mathbf{A}_2^{ext} - \Phi'_2).\end{aligned} \tag{A.29}$$

Now we insert equation (2.37a) into (A.28) and (A.29) and use

$$\begin{aligned}\mathbf{H}_1\,\mathbf{h}_1 &= \mathbf{H}_1\,G_1^{-1}(G_2\,\mathbf{h}_2 + \Delta\,\mathbf{A}_{ext}) = \Sigma_1(G_2\,\mathbf{h}_2 + \Delta\,\mathbf{A}_{ext}),\\ \mathbf{H}_2\,\mathbf{h}_2 &= \mathbf{H}_2\,G_2^{-1}(G_2\,\mathbf{h}_2) = \Sigma_2(G_2\,\mathbf{h}_2 + \Delta\,\mathbf{A}_{ext}),\end{aligned} \tag{A.30}$$

with the notation $\Sigma_{1,2} = \mathbf{H}_{1,2}\,G_{1,2}^{-1}$. In the following we will also use

$$\mathbf{H}_1\,\epsilon_1\sigma_1 = \Sigma_1 L_1 G_1\sigma_1 \quad , \quad L_{1,2} = G_{1,2}\epsilon_{1,2}G_{1,2}^{-1}$$

after some calculating we arrive at

$$\begin{aligned}(\Sigma_1 - \Sigma_2)G_2\,\mathbf{h}_2 - ik\,\hat{\mathbf{n}}(L_1 - L_2)G_2\sigma_2 = \\ \Delta\,\mathbf{A}'_{ext} + ik\,\hat{\mathbf{n}}(\epsilon_1\Phi_1 - \epsilon_2\Phi_2) - \Sigma_1\Delta\,\mathbf{A}_{ext} + ik\,\hat{\mathbf{n}}\,L_1\Delta\Phi_{ext},\\ (\Sigma_1 L_1 - \Sigma_2 L_2)G_2\sigma_2 - ik\,\hat{\mathbf{n}}(L_1 - L_2)G_2\,\mathbf{h}_2 = \\ D'_e - \Sigma_1 L_1\Delta\Phi_{ext} + ik\,\hat{\mathbf{n}}\cdot L_1\Delta\,\mathbf{A}_{ext}\,.\end{aligned}$$

With the following abbreviations used

$$\begin{aligned}D_e &= D'_e - \Sigma_1 L_1\Delta\Phi_{ext} + ik\,\hat{\mathbf{n}}\cdot L_1\Delta\,\mathbf{A}_{ext},\\ D'_e &= \epsilon_1(ik\,\hat{\mathbf{n}}\cdot\mathbf{A}_1^{ext} - \Phi'_1) - \epsilon_2(ik\,\hat{\mathbf{n}}\cdot\mathbf{A}_2^{ext} - \Phi'_2),\end{aligned}$$

$$
\begin{aligned}
\vec{\alpha} &= \vec{\alpha}' - \Sigma_1 \Delta\, \mathbf{A}_{ext} + ik\, \hat{\mathbf{n}}\, L_1 \Delta \Phi_{ext}, \\
\vec{\alpha}' &= \Delta\, \mathbf{A}'_{ext} + ik\, \hat{\mathbf{n}} (\epsilon_1 \Phi_1 - \epsilon_2 \Phi_2), \\
\Sigma &= \Sigma_1 L_1 - \Sigma_2 L_2 + k^2\, \hat{\mathbf{n}} \cdot (L_1 - L_2) \Delta^{-1}\, \hat{\mathbf{n}} (L_1 - L_2), \\
\Delta &= \Sigma_1 - \Sigma_2.
\end{aligned}
$$

A.7. Derivation of far field radiation

The following schematic describes the determination of the vector potential in the far field. The integrals defining $\mathbf{A}$ simplify in the far field because the vectors $\mathbf{r}$ and $\mathbf{r} - \mathbf{r}'$ become nearly parallel.

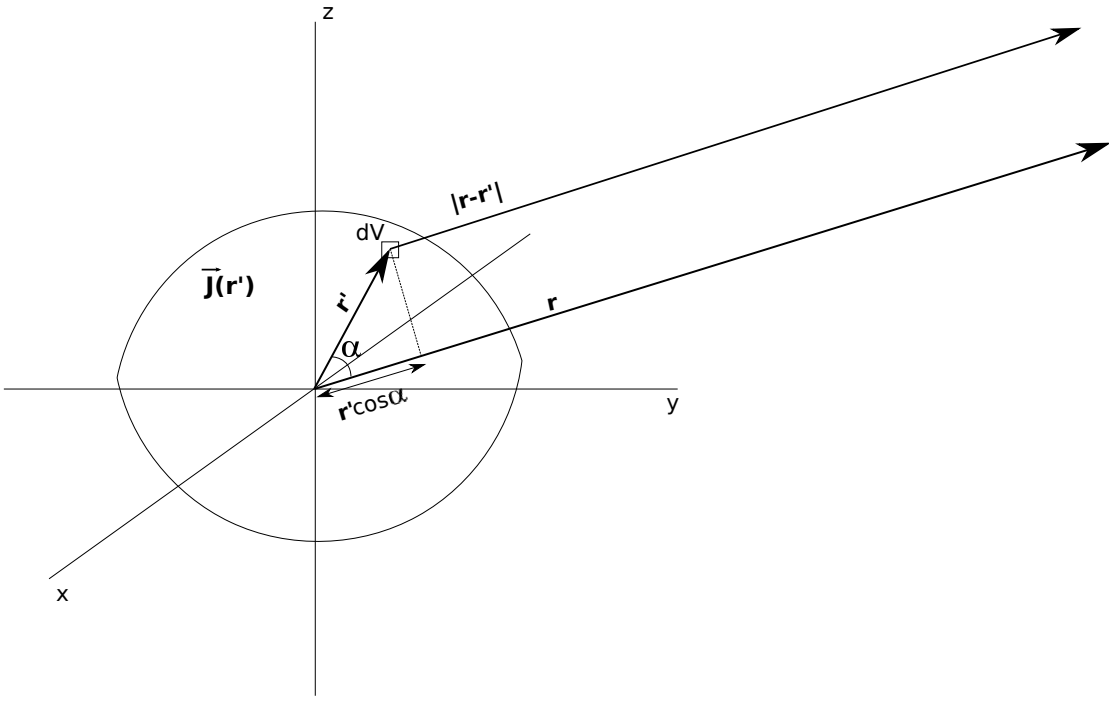

Figure A.2.: Vector schematic for the radiation of an arbitrary body with a surface current $\mathbf{j}(\mathbf{r}')$.

We can make the approximation

$$
|\, \mathbf{r} - \mathbf{r}' \,| \simeq r - r' \cos\alpha. \tag{A.31}
$$

Therefore the integrand of equation (2.40) yields

$$\frac{e^{-ik|\,\mathbf{r}-\mathbf{r}'\,|}}{|\,\mathbf{r}-\mathbf{r}'\,|} \simeq \frac{e^{-ikr}e^{ikr'\cos\alpha}}{r - r'\cos\alpha}, \tag{A.32}$$

and if we now assume that $r \gg r'$, which is valid in the far field region, the denominator of equation (A.32) can be simplified to give

$$\frac{e^{-ik|\,\mathbf{r}-\mathbf{r}'\,|}}{|\,\mathbf{r}-\mathbf{r}'\,|} \simeq \frac{e^{-ikr}e^{ikr'\cos\alpha}}{r}. \tag{A.33}$$

The r'-term in the numerator complex exponential term of equation (A.33) represents the phase shift that is still significant in the far field, hence it cannot be omitted.
The r-dependent terms can now be taken out of the integral because we only need to integrate over r'.

$$\mathbf{A}(\mathbf{r}) \simeq \mu\frac{e^{-ikr}}{4\pi r}\int_V \mathbf{j}(\mathbf{r}')e^{ikr'\cos\alpha}dV \tag{A.34}$$

It is useful to establish the following equality

$$|\,\mathbf{r}-\mathbf{r}'\,| \simeq r - r'\cos\alpha = r - r'\,\hat{\mathbf{n}}, \tag{A.35}$$

with $\hat{\mathbf{n}}$ being the normal vector on the surface of the body.

A.8. Derivation of the extinction cross section

The knowledge of the electromagnetic far field allows for the calculation of the optical characteristics of the scattering particle. The extinction cross section C^{ext} is the sum of the scattering and absorption cross sections and, when multiplied by the incident monochromatic energy flux, gives the total monochromatic power removed from the incident light by the combined effect of scattering and absorption [19].

When we assume that the medium surrounding the scattering particle is non-absorbing, the net rate at which the electromagnetic energy crosses a surface of a sphere S around the object, with a large enough radius r to be in the far-field zone, is always non-

negative and equal to the power absorbed by the particle

$$W^{abs} = -\int_S dS\langle \mathbf{S}(\mathbf{r})\rangle \cdot \hat{\mathbf{r}} = -r^2 \int_{4\pi} d\hat{\mathbf{r}}\langle \mathbf{S}(\mathbf{r})\rangle \cdot \hat{\mathbf{r}}. \tag{A.36}$$

The absorption can be written as

$$W^{abs} = W^{inc} - W^{sca} + W^{ext}. \tag{A.37}$$

where,

$$W^{inc} = -r^2 \int\limits_{4\pi} d\hat{\mathbf{r}}\langle \mathbf{S}^{inc}(\mathbf{r})\rangle \cdot \hat{\mathbf{r}}, \quad W^{sca} = -r^2 \int\limits_{4\pi} d\hat{\mathbf{r}}\langle \mathbf{S}^{sca}(\mathbf{r})\rangle \cdot \hat{\mathbf{r}}, \tag{A.38}$$

$$W^{ext} = -r^2 \int\limits_{4\pi} d\hat{\mathbf{r}}\langle \mathbf{S}^{ext}(\mathbf{r})\rangle \cdot \hat{\mathbf{r}}. \tag{A.39}$$

S^{inc} is constant because of the non-absorbing surrounding medium and therefore W^{inc} vanishes. W^{inc} is the rate at which the scattered energy crosses the surface S in outward direction. It follows now that W^{ext} is the sum of the energy scattering and absorption rate $W^{ext} = W^{sca} + W^{abs}$. Combining equations (A.39), (5.1) and the definition of the respective fields

$$\mathbf{E}^{inc}(\mathbf{r}) = \mathbf{E}_0^{inc}\, e^{ik\,\hat{\mathbf{n}}^{inc}\cdot\mathbf{r}} \tag{A.40}$$

$$\underset{kr\to\infty}{=} \frac{i2\pi}{k}\left[\delta(\hat{\mathbf{n}}^{inc}+\hat{\mathbf{r}})\frac{e^{ikr}}{r} - \delta(\hat{\mathbf{n}}^{inc}-\hat{\mathbf{r}})\frac{e^{ikr}}{r}\right]\mathbf{E}_0^{inc}, \tag{A.41}$$

$$\mathbf{H}^{inc}(\mathbf{r}) = \sqrt{\frac{\epsilon}{\mu_0}} e^{ik\,\hat{\mathbf{n}}^{inc}\cdot\mathbf{r}}\,\hat{\mathbf{n}}^{inc}\times\mathbf{E}_0^{inc} \tag{A.42}$$

$$\underset{kr\to\infty}{=} \frac{i2\pi}{k}\left[\delta(\hat{\mathbf{n}}^{inc}+\hat{\mathbf{r}})\frac{e^{ikr}}{r} - \delta(\hat{\mathbf{n}}^{inc}-\hat{\mathbf{r}})\frac{e^{ikr}}{r}\right]\sqrt{\frac{\epsilon}{\mu_0}}\,\hat{\mathbf{n}}^{inc}\times\mathbf{E}_0^{inc}, \tag{A.43}$$

$$\mathbf{E}^{sca}(\mathbf{r}) \underset{kr\to\infty}{=} \frac{e^{ikr}}{r}\mathbf{E}^{sca}, \tag{A.44}$$

$$\mathbf{H}^{sca}(\mathbf{r}) \underset{kr\to\infty}{=} \sqrt{\frac{\epsilon}{\mu_0}}\frac{e^{ikr}}{r}\hat{\mathbf{r}}\times\mathbf{E}^{sca}(\hat{\mathbf{r}}). \tag{A.45}$$

we arrive at the extinction cross section

$$C^{ext} = \frac{W^{ext}}{\frac{1}{2}\sqrt{\epsilon/\mu_0}|\,\mathbf{E}_0^{inc}\,|^2} = \frac{4\pi}{k|\,\mathbf{E}_0^{inc}\,|^2}\Im\left[\mathbf{E}^{sca}(\hat{\mathbf{n}}^{inc})\cdot\mathbf{E}_0^{inc*}\right]$$
$$= \frac{4\pi}{k\mathcal{E}_0^{inc}}\Im\left[\hat{\mathbf{x}}\cdot\mathbf{E}_1^{sca}(\hat{\mathbf{n}}^{inc})\right]$$

This shows that the extinction results from the interference between the incident and scattered light.

Bibliography

[1] U. Hohenester and A. Trügler. MNPBEM - a matlab toolbox for the simulation of plasmonic nanoparticles. *Comp. Phys. Commun.*, 183, 2012.

[2] F. J. García de Abajo and A. Howie. Retarded field calculation of electron energy loss in inhomogeneous dielectrics. *Phys. Rev. B*, 65:115418, Mar 2002.

[3] M.L. Brongersma and P.G. Kik. *Surface Plasmon Nanophotonics*. Springer series in optical sciences. Springer, 2007.

[4] Harry A. Atwater. The Promise of Plasmonics. *Sci Am*, 296(4):56–62, April 2007.

[5] John David Jackson. *Classical electrodynamics*. Wiley, New York, NY, 3rd ed. edition, 1999.

[6] L. Novotny and B. Hecht. *Principles of Nano-Optics*. Cambridge University Press, 2011.

[7] L. Lorenz. On the identity of the vibrations of light with electrical currents. *Philos. Mag. 34*, pages 287–301, 1867.

[8] C. Hafner. *The Generalized Multipole Technique for Computational Electromagnetics*. The Artech House Antenna Library. Artech House., 1990.

[9] U. Hohenester and A. Trügler. *Optical Properties of Metallic Nanoparticles: Introduction and Basic Principles*. Springer, 2012.

[10] G. Mie. Beiträge zur Optik trüber Medien, speziell kolloidaler Metallösungen. *Annalen der Physik*, 330:377–445, 1908.

[11] Andreas Trügler. Optical properties of metallic nanoparticles. *PhD thesis, Karl-Franzens Universität Graz*, July 2011.

[12] F. J. García de Abajo. Optical excitations in electron microscopy. *Rev. Mod. Phys.*, 82:209–275, Feb 2010.

[13] Amit Chakrabarti Matthew J.Berg, Christopher M. Sorensen. Extinction and the electromagnetic optical theorem. *Journal of the Optical Society of America A (JOSA A)*, 25:1504, 2008.

[14] M. Born, E. Wolf, A.B. Bhatia, P.C. Clemmow, D. Gabor, A.R. Stokes, A.M. Taylor, P.A. Wayman, and W.L. Wilcock. *Principles of Optics: Electromagnetic Theory of Propagation, Interference and Diffraction of Light*. Cambridge University Press, 1999.

[15] E.D. Palik. *Handbook of Optical Constants of Solids, Volumes I, II, and III: Subject Index and Contributor Index*. Academic Press Handbook Series. Elsevier Science & Tech, 1985.

[16] B. Lamprecht, G. Schider, R. T. Lechner, H. Ditlbacher, J. R. Krenn, A. Leitner, and F. R. Aussenegg. Metal nanoparticle gratings: Influence of dipolar particle interaction on the plasmon resonance. *Phys. Rev. Lett.*, 84:4721–4724, May 2000.

[17] M. Meier, A. Wokaun, and P. F. Liao. Enhanced fields on rough surfaces: dipolar interactions among particles of sizes exceeding the rayleigh limit. *J. Opt. Soc. Am. B*, 2(6):931–949, Jun 1985.

[18] Weng Cho Chew. *Waves and Fields in Inhomogeneous Media (Electromagnetic Waves)*. IEEE Computer Society Press, 1995.

[19] M.I. Mishchenko, L.D. Travis, and A.A. Lacis. *Scattering, Absorption, and Emission of Light by Small Particles*. Cambridge University Press, 2002.